Bioresource Technology 440 (2026) 133413

Contents lists available at ScienceDirect

Bioresource Technology

journal homepage: www.elsevier.com/locate/biortech

Novel continuous production of single-cell proteins from purple non-sulfur bacteria using gaseous volatile fatty acids by closed-loop membrane contactor system

Riccardo Lo Coco, Marco Pezzuto, Aleksandra Jelic, Stefano Cazzaniga, Nicola Frison *

Department of Biotechnology, University of Verona, Strada Le Grazie 15, 37134 Verona, Italy

HIGHLIGHTS

- Membrane-mediated gaseous VFA feeding prevents direct contact with PNSB biomass.
- VFA mass flux up to 8.9 gCOD·m^{-2}·h^{-}1 enabled efficient carbon transfer.
- The PNSB biomass contained 62% crude protein and 1.5% pigments.
- Amino acidic profile supports PNSB biomass as alternative aquafeed ingredient.

GRAPHICAL ABSTRACT

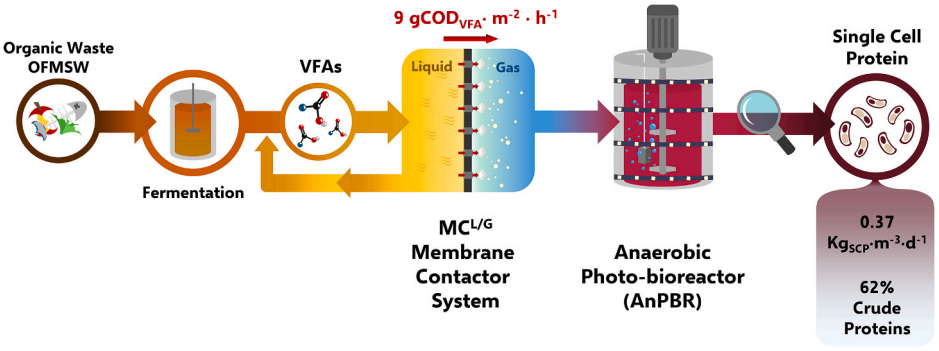

ARTICLE INFO

Keywords:
Acidogenic fermentation
Membrane technology
Alternative feed ingredients
Resource recovery
Biorefinery

ABSTRACT

This study explores the continuous cultivation of purple non-sulfur bacteria (PNSB) in an anaerobic photo-bioreactor (AnPBR) to produce single-cell protein (SCP) and other valuable co-products, such as pigments and polyhydroxyalkanoates (PHAs), using a gaseous stream of volatile fatty acids (VFA) transferred from a synthetic mixture (70 % acetic, 10 % propionic, 20 % butyric acid; 13.6 ± 1.6 gCOD·L^{-1}; pH 3.0 ± 0.1) using a closed-loop membrane contactor system. This approach avoids the direct contact between the fermented broth containing

Abbreviations: A, Membrane Surface Area; [A]I, Concentration of VFA Anion; AnPBR, Anaerobic PhotoBioreactor; BChl, Bacteriochlorophyll; COD, Chemical oxygen demand; CP, Crude Protein; Crts, Carotenoids; CS, Chemical score; DO, Dissolved oxygen; EAA, Essential Amino Acids; EU, European Union; HAc, Acetic acid; [HA]I, Concentration of Undissociated VFA; HBu, Butyric acid; HPr, Propionic acid; HRT, Hydraulic Retention Time; j, VFA Flux; Ke, Experimental Overall Mass Transfer Coefficient; LHC, Light-harvesting complex; MC, Membrane Contactor; mi,F,0, Initial Mass of VFA in the Feed; mi,F,t, Mass of VFA in the Feed at Time t; mi, S, Mass of VFA in the Stripping Solution at the End of the Experiment; MLVSS, Mixed Liquor Volatile Suspended Solids; n° cycle, Number of Cycles; NIR, Near-infrared; OFMSW, Organic fraction of municipal solid waste; OLR, Organic Loading Rate; ORP, Oxidation-reduction potential; PHA, Polyhydroxyalkanoates; pKa, Acid Dissociation Constant; PNSB, Purple non-sulfur Bacteria; Q, Flow Rate; Ri, Overall VFA Recovery Efficiency; SBR, Sequencing Batch Reactor; SCP, Single-Cell Protein; SDG, Sustainable development goals; SRT, Sludge Retention Time; Ti, Transfer Efficiency; VFA, Volatile Fatty Acids; Vfeed, Volume of the Feed Solution; [VFA]F, t (VFA Concentration on the Feed Side at Time t; [VFA]S, t (VFA Concentration on the Stripping Side at Time t; tc,cycle, Contact Time of a Single Feed Cycle; VMC, Volume of the MC Shell; tc,tot, Total Contact Time.

* Corresponding author.
E-mail addresses: riccardo.lococo@univr.it (R. Lo Coco), marco.pezzuto@univr.it (M. Pezzuto), aleksandra.jelic@univr.it (A. Jelic), stefano.cazzaniga@univr.it (S. Cazzaniga), nicola.frison@univr.it (N. Frison).

https://doi.org/10.1016/j.biortech.2025.133413
Received 14 May 2025; Received in revised form 10 September 2025; Accepted 27 September 2025
Available online 29 September 2025

VFA and the cultivated biomass. Over 160 days of operation, the system was optimized across four experimental periods to evaluate the impact of varying organic loading rates (OLRs) on biomass yield and quality. During the fourth period, the membrane contactor (MC) operated with a total contact time of 1.92 min and a stripping time of 4 h at a feed temperature of 32 ± 1°C, achieving a VFA mass flux of 8.86 $gCOD \cdot m^{-2} \cdot h^{-1}$ and supporting an OLR of 3.9 ± 0.8 $gCOD \cdot L^{-1} \cdot d^{-1}$. Under these conditions, the AnPBR achieved a biomass production rate of 0.36 ± 0.01 $kgX_{PB} \cdot m^{-3} \cdot d^{-1}$, with a crude protein content of 62 % and an amino acid profile that met the dietary requirements of aquaculture species. Additionally, the photoheterotrophic metabolism of PNSB enabled the co-production of pigments and polyhydroxyalkanoates (PHAs), adding nutritional and economic value to the biomass. This study highlights the potential of the MC-AnPBR system for sustainable, high-quality SCP production, contributing to circular bioeconomy goals and supporting sustainable aquaculture practice.

1. Introduction

Protein is a key macronutrient for human and animal nutrition. However, the European Union's heavy reliance on imported sources exposes the market to volatility and food security risks. The protein feed market is expanding rapidly (it was valued at €14.9 billion in 2023 and is projected to reach €28.5 billion by 2032), and global demand for meat protein is expected to rise by 14 % this decade (Adesogan et al., 2020). This growing demand puts pressure on conventional feed ingredients such as soybeans, cereals and fishmeal, the supply of these ingredients is further challenged by geopolitical instability, the ongoing effects of the 2019–2020 pandemic, depletion of natural resources, loss of biodiversity and climate change (Pesante et al.,2024).

One such solution is single-cell protein (SCP) production, a biotechnological approach that offers scalable, affordable, and environmentally sustainable protein sources (Allegue et al., 2022). SCP is derived from microorganisms such as yeasts, fungi, algae, and bacteria that can grow on diverse carbon sources (Hülsen et al., 2022b). Among these, purple non-sulfur bacteria (PNSB) have garnered particular interest due to their ability to grow under anaerobic conditions and efficiently convert organic substrates like volatile fatty acids (VFAs) from waste streams into valuable bioproducts such as SCP (Capson-Tojo et al., 2020a).

PNSB biomass has high protein content (50–60 %) which makes it ideal to use as SCP and in the presence of value-added compounds such as pigments (including carotenoids) or polyhydroxyalkanoates, these compounds offer enhanced nutritional value (Hülsen et al., 2022b; Pesante et al., 2024). Carotenoids, known for their antioxidant properties and applications in pharmaceuticals, food, cosmetics and biofuels, are an important by-product. Unlike synthetic alternatives, carotenoids from natural sources are safer and more sustainable, making PNSB biomass suitable for SCP production (Ángeles et al., 2025).

PNSB biomass has been suggested as an ingredient for producing sustainable and cost-effective protein feed in the form of fishmeal (Alloul et al., 2021; Delamare-Deboutteville et al., 2019). Using anaerobic and phototrophic bacteria for SCP production also results in a lower energy demand (450 versus 4000 MJ/kg *N*-protein) than conventional processes (Matassa et al., 2015). Furthermore, PNSB can utilise organic waste streams, such as fermentation effluents, without competing with other phototrophs by utilising near-infrared light (NIR) to facilitate the absorption of compounds such as VFAs (Pikaar et al., 2017).

Volatile fatty acids (VFAs) such as acetate, propionate, and butyrate are short-chain fatty acids obtained from anaerobic fermentation of organic waste (Strazzera et al., 2018). Through the carboxylate platform, they can be recovered and valorised into multiple products (Lo Coco et al., 2024). Acetate plays a central role by enhancing the uptake of propionate and butyrate and accelerating PNSB growth, thereby improving carbon utilisation, protein content, and biomass yield. Mixtures with high acetate content also stimulate pigments production compared to propionate or butyrate alone (Hülsen et al., 2022b). Thus, VFAs serve not only as carbon substrates but also as enhancers of PNSB growth and SCP yield, highlighting their potential in sustainable SCP production

VFAs are increasingly recognised as a renewable source of carbon with applications in wastewater treatment, phosphorus recovery, biofuels and bioplastics (Pervez et al., 2022). They are essential substrates for SCP production, highlighting their growing importance in the food, feed and bioplastics sectors (Allegue et al., 2022). However, separating and purifying VFAs from complex fermentation effluents remains a major challenge for large-scale production (Pervez et al.,2022). Efficient recovery is crucial to secure their use in SCP and to prevent acid-induced microbial stress. Several separation techniques, such as distillation, adsorption, solvent extraction, ion-exchange, and membrane-based technologies, have been developed to address this issue (Atasoy et al., 2018; Pervez et al., 2022). Using extracted VFAs simplifies the composition of the feedstock and avoids the variability typical of sewage. Membrane-based systems not only improve separation efficiency, but also act as a barrier against pathogens, providing safer substrates for microbial cultivation. (Alloul et al., 2018).

However, cultivating PNSB on waste streams can be challenging due to the dilution of PNSB biomass within complex microbial consortia and the potential presence of pathogens (Allegue et al., 2022; Wada et al., 2022). These contamination risks limit the direct use of PNSB biomass from waste-fed systems as a protein source in aquaculture, which highlights the advantages of using extracted VFAs as a safer alternative. Among these, membrane contactors (MC) have shown significant promise due to their operational flexibility, cost-effectiveness, and environmental benefits (Aydin et al., 2018; Hasanoğlu et al., 2010). In most reported applications, hollow-fibre membrane contactors have been employed in liquid–liquid configurations for the recovery and purification of VFAs from fermentation broths (Lo Coco et al., 2024; Tugtas, 2014a). These technologies facilitate the recovery of VFAs without using high pressure or size exclusion mechanisms, making them ideal for increasing SCP production using waste-derived VFAs.

Hollow-fibre membrane contactors (MCs) facilitate gas transfer without direct phase contact, thereby preventing issues such as foaming and flooding (Pervez et al.,2022). Gas transfer is driven by a pressure differential, enabling VFAs to efficiently move into the gas phase and be supplied to microbial cultures. MCs can operate under vacuum to yield a pure gas stream or in sweep gas mode to produce diluted mixtures, the latter being more energy-efficient (Aydin et al., 2018). For SCP production, vacuum operation has the advantage of providing a controlled, high-purity gas stream that is ideal for use as a feed.

The integration of PNSB into SCP is in line with key EU sustainability initiatives, including the Waste Framework Directive (2008/98/EC) and the Circular Economy Action Plan, both of which prioritize the recovery and reuse of resources from waste streams to reduce environmental impact. PNSBs have a high carbon and nutrient assimilation efficiency (optimal COD:N:P uptake ratio of 100:5:1 with > 90 % carbon-nutrient assimilation) (Capson-Tojo et al., 2021), converting waste into microbial biomass by high growth yield, reducing the waste and environmental footprint of protein production. This directly contributes to the EU's efforts to promote a circular economy and sustainability in all sectors. Additionally, coupling AnPBR with hollow-fibre membrane contactor (MC) technology improves the efficient transfer of VFA in gaseous form into the bioreactor, optimizing microbial growth and SCP yield.

Building on the well-established role of VFAs as substrates for PNSB, this study introduces a novel configuration in which VFAs are delivered

in gaseous form via a hollow-fibre membrane contactor. This approach avoids direct liquid contact with fermentation effluents, reducing contamination risks and improving SCP biomass quality. This study will be established for proof-of-concept studies. The objectives of the study are to (i) optimise the operating conditions within the MC-AnPBR setup to maximise VFA transfer rates; (ii) assess the impact of organic loading rate (OLR) at the same hydraulic retention time (HRT) on PNSB biomass production and pigment, protein and overall biomass yield; and (iii) determine the scalability potential of this approach for continuous in-line cultivation of PNSB suitable for SCP production.

2. Materials and methods

2.1. Production of purple non-sulfur bacteria via volatile fatty acids gas system

A synthetic volatile fatty acids (VFA) mixture (2 L) was prepared daily as the feed solution for the MC experiments. The mixture had concentration of 13600 ± 1600 mgCOD·L^{-1}, consisting of 70 % acetic acid, 10 % propionic acid, and 20 % butyric acid. The VFA concentration ratio in the synthetic mixture corresponded to the typical VFA composition of the fermentation broths obtained from organic-rich wastes (OFMSW) as reported by (Righetti et al., 2020; Strazzera et al., 2018). The initial pH of the feed solution was 3.0 ± 0.1. The ionic strength of the synthetic VFA solution was relatively low compared to real waste-

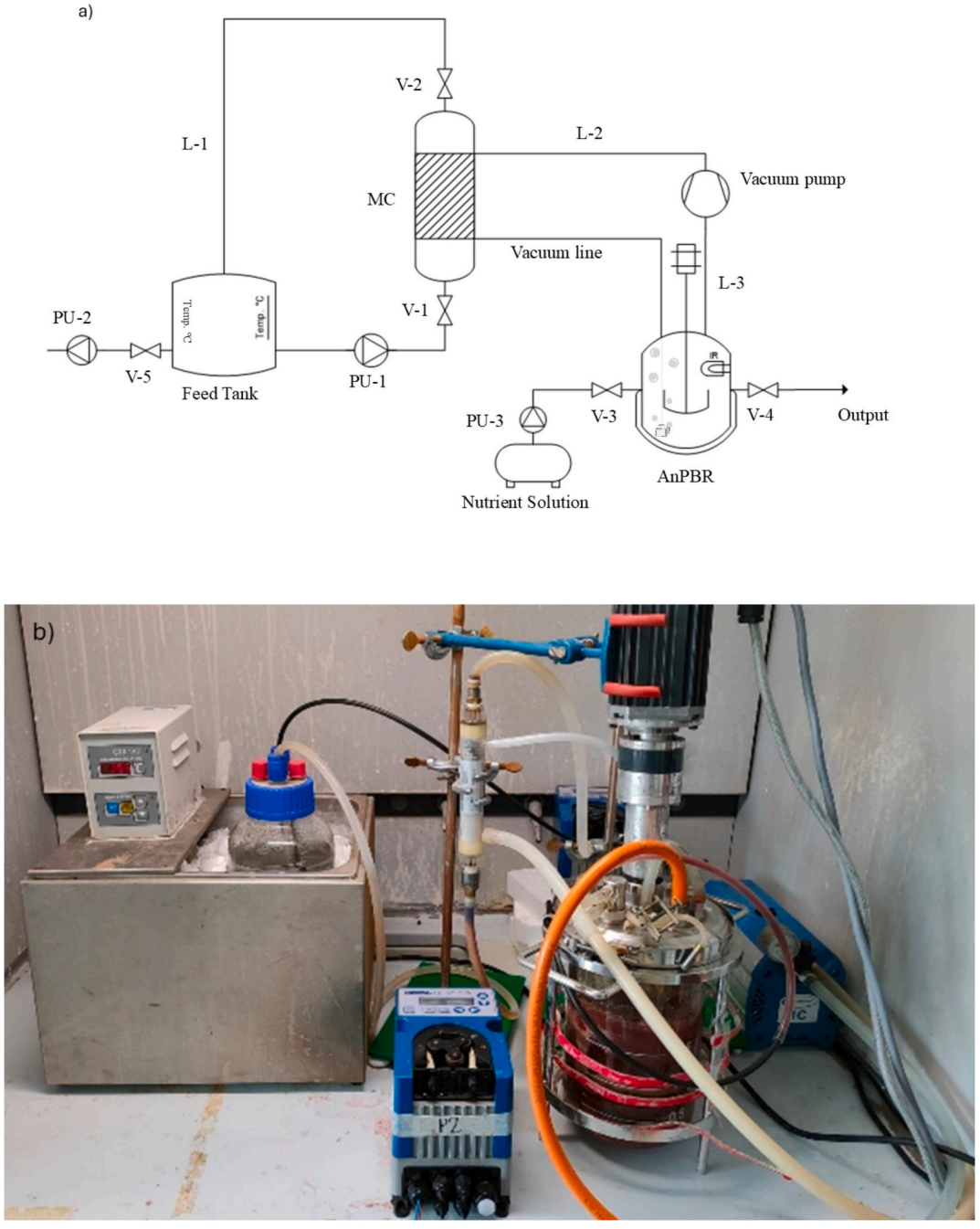

Fig. 1. a) Process flow diagram of MC-AnPBR system; MC = Membrane contactor; AnPBR = Anaerobic photobioreactor. PU = Pumps; L = Pipelines; V = Valves; IR = Illumination system (near-infrared light source) b) setup used during experimental period.

derived effluents, in which dissolved salts substantially contribute to osmotic pressure. Differences in ionic strength can affect VFA transfer across the membrane contactor, since higher ionic strength is known to alter osmotic gradients and retention behaviour. This can potentially reduce the overall transfer efficiency (Pervez et al., 2022).

Fig. 1 illustrates the process flow diagram of the setup used to study the separation and gas-phase transfer of VFAs directly into the bioreactor for the growth of PNSB open culture. The system consists of two separate units: a MC for the separation of VFA (gaseous stream) from a feed solution, which serve as carbon source for the photoheterotrophic growth of PNSB in a subsequent AnPBR (Fig. 1). The MC setup utilized a microporous polypropylene hollow fibre MC module 3 M™ Liqui-Cel™ MM-1x5.5 Series, Italy, with an internal surface area of 0.22 m^2 (see supporting material).

The selected porosity (30–40 %) and pore size (between 0.03 μm and 0.2 μm) aim to prevent bacterial contamination from the feed tank, which are typically larger than 0.2 μm (3 M Operating conditions and protocols). The MC was connected to a VFA feed solution on the lumen side. The solution was continuously mixed to ensure rapid equilibration before being recirculated back to the MC. The synthetic mixture of VFA was continuously recirculated through the membrane using a peristaltic pump (Kronos 50, SEKO) at a flow rate of 225 mL·min^{-1} in closed-loop mode based on the previous study of (Lo Coco et al., 2024). The operating temperature of the MC was maintained using a temperature-controlled chamber (GTR 190, Thermoregulation). The system was operated at controlled temperatures of 20 ± 1 °C, 25 ± 1 °C, and 32 ± 1 °C depending on the experimental period (Table 1).The MC system was thoroughly cleaned between each experimental set using filtered, dechlorinated, and deionized water for 30 min. Although membrane fouling, wetting, and degradation are recognised as possible operational issues during long-term use, these aspects were not the primary focus of the present study.

The transfer of VFAs from the feed tank through the MC system and into the AnPBR (via Teflon tubing connected to the shell side of the MC) (Fig. 1) was facilitated by a vacuum pump (VacuumBrand 1C, 50/60 Hz, 0.7/0.85 m^3 h^{-1}) which maintained a constant pressure of 0.1 bar. Furthermore, at the start of the experiment, the headspace of the reactor was purged with nitrogen to create anaerobic conditions, then a vacuum was applied to create and maintain the operating pressure throughout the entire experimental period. The operating pressure was selected following the MC manufacturer's guidelines (3 M Liquid-Cell MM series) to minimise water evaporation (0.05–0.08 bar at 20 °C) and to enhance equipment longevity (0.04–0.2 bar). The applied vacuum creates a partial pressure differential between the liquid phase (lumen) and the gas phase (shell), which drives the transfer of dissolved gases from the lumen side to the shell side. The system operated as a closed headspace–membrane loop, in which VFAs were stripped from the feed solution by an headspace stream circulating through the membrane contactor and reintroduced into the photobioreactor via a sparger. Additionally, the vacuum pump facilitates the transfer of the VFA gaseous stream from the MC into the AnPBR, while also helping to maintain anaerobic conditions within the bioreactor. Driven by vacuum, the VFA gaseous stream from the MC was sparged into the AnPBR through a porous ceramic diffuser (5 x 3 x 3 cm), immersed at a depth of 14 cm of the bioreactor. Such MC-AnPBR system design prevents direct contact between the PNSB biomass and the feed solution, thereby reducing the risk of cross-contamination.

2.2. Anaerobic photobioreactor unit

2.2.1. Inoculum

A *Rhodopseudomonas palustris* (*R. palustris* sp.) (DSM 126) purchased from the German Collection of Microorganisms and Cell Cultures (DSMZ, Braunschweig, Germany) was used in this study. The inoculum was cultivated in 2L Schott bottles which were fed with modified medium for *Rhodospirillaceae (German Collection of Microorganisms and cell cultures GmbH_DSMZ: https://www.dsmz.de)*. The composition of the modified medium and of the trace element is reported in section 2.4.2 The Schott bottle was illuminated with NIR light, stirred magnetically and incubated at 30 °C under anaerobic conditions. The pH was adjusted to 7.0 by adding NaOH 1 M. Finally, the medium was sterilized at 120 °C for 15 min. The pure culture of *R. palustris* sp. was cultivated in the modified medium for *Rhodospirillaceae* until it reached a concentration of 1.0–1.2 gVSS•L^{-1} (after about 5 days). The resulting PNSB culture into the AnPBR at a concentration of 0.75 ± 0.08 gVSS•L^{-1} to avoid the lag-phase and ensure a rapid and stable PNSB growth response in the bioreactor. Although the inoculum consisted of a pure culture of *Rhodopseudomonas palustris*, the AnPBR was operated under open-culture conditions, thus allowing the coexistence of other microorganisms. This choice was intended to test the robustness of PNSB cultivation in non-sterile environments, where their selective advantage can be exploited (Hülsen et al., 2020).

2.2.2. Anaerobic photobioreactor configuration and operations

Fig. 1 shows the AnPBR as the second unit of the system. Specifically, the AnPBR was operated as Sequencing Batch Reactor (SBR) for 160 days and it is fed through VFAs transferred via gas by the MC (Unit 1). A 3 L cylindrical AnPBR with working volume of 2L was equipped with a submerged diffuser for the transfer of VFA into the mixed liquor which represent the only source of carbon. The width and the height of the AnPBR were respectively 17 and 21 cm and the water height was of 16.5 cm. The bioreactor was equipped with a submerged diffuser to transfer the gaseous VFA stream into the PNSB culture medium and with a mixer (Heidolph Constant-Speed Mixer) for continuous stirring at 230 rpm. The bioreactor was connected to the MC system on one side and to a vacuum pump on the other, which enabled a continuous and controlled

Table 1
Experimental periods and operating conditions of the MC system.

	Vacuum (mbar)	Flow rate (mL•min^{-1})	Stripping time (h)	$t_{c,tot}$ (min)	Temperature (°C)	$OLR_{applied}$ (gCOD•$L^{-1}d^{-1}$)	Min-Max (gCOD•$L^{-1}d^{-1}$)
Preliminary test and start −up (0-10d)	100	225	2; 4; 6; 9	0.96; 1.92; 2.88; 4.32	Room temperature (18–22)	0.2 ± 0.01; 1.0 ± 0.1; 1.4 ± 0.1; 1.8 ± 0.2	0.15–0.22 0.91–1.2 1.2–1.63 1.55–2.04
PERIOD 1 (11-23d)	100	225	4	1.92	20 ± 1	0.7 ± 0.2	0.55–0.95
PERIOD 2 (28-43d)	100	225	6	2.88	20 ± 1	1.3 ± 0.3	0.99–1.8
PERIOD 3 (44-63d)	100	225	6	2.88	25 ± 1	1.9 ± 0.3	1.52–2.35
PERIOD 4.1 (64-76d)	100	225	6	2.88	32 ± 1	5.8 ± 0.6	5.02–6.53
PERIOD 4.2 (78-160d)	100	225	4	1.92	32 ± 1	3.9 ± 0.8	3.08–4.92

supply of VFAs in gaseous form into the liquid phase of the bioreactor (see section 2.3) (Fig. 1). The AnPBR was illuminated at 31.7 $W{\cdot}m^{-2}$ with NIR light (LuxaLight LED-strip 24 V Infra-red Protected 2835) with a wavelength of 810–870 nm (see supporting material), chosen based on the absorption peaks of Bacteriochlorophyll (BChl) (Capson-Tojo et al., 2021). In particular, the applied NIR illumination enables selective enrichment of PNSB by avoiding competition with other phototrophic biomasses to favour photoheterotrophic PNSB growth (Pikaar et al., 2017). The illuminated surface/volume ratio was 40 $m^2{\cdot}m^{-3}$. The temperature of the AnPBR was maintained at 30 ± 2°C, which is within the optimal growth range for PNSB, using a temperature control system. The pH of the mixed liquor was maintained at 7.5 ± 0.2 throughout the experiments by adding non-sterilized nutrient solution into the AnPBR, which was alkalinized by adding 1 M NaOH, to keep the pH within the optimal range for the PNSB growth. The nutrient solution had the composition of the modified medium for *Rhodospirillaceae* used for the inoculum preparation, except for the carbon sources (Disodium succinate, Ammonium acetate). The organic carbon source for the PNSB growth were solely the VFAs transferred via MC from the feed solution at given organic loading rates. The bubbling generated by the VFA gas flowing in through the diffuser enhances the microbial uptake of VFAs, which solubilize and become readily available for PNSB at the pH of the mixed liquor – pH 7.5 ± 0.4 – (pH > pKa(VFA): RCOOH > $RCOO^-$). Moreover, the bubbling creates localised shear forces that aids the biofilm removal forming on the reactor surfaces. According to (Huang et al., 2025), the AnPBR was operated at a sludge retention time (SRT) of 5 days (equal to the HRT) by removing the 20 % of the reactor volume and adding the same volume daily with the nutrient solution (without adding the organic carbon source). The nutrient solution was introduced using a peristaltic pump (Kronos 50, SEKO) at a flow rate of 225 $mL{\cdot}min^{-1}$. The AnPBR run through three main phases per day sequentially: (1) Reactor feeding phase, whereby the nutrient solution was supplied for about 3 min and subsequently the VFAs (gaseous stream) from the MC was supplied to the reactor for 4–6 h (stripping) depending on the operating period ($t_{stripping}$, see Table 1); (2) Reaction phase lasts 15–18 h which represent the fraction of the cycle where MC was not operated ($t_{post\text{-}stripping}$), and (3) Discharge phase ($t_{effluent}$ ~ 3 min), according to the fixed SRT (5 days). During the experiments, samples were collected during each step in both the feed solution and AnPBR to study the performance of the process. Additionally, pH and conductivity of the feed solution, as well as pH, conductivity, and oxidation–reduction potential (ORP) of the AnPBR reactor, were regularly monitored to evaluate process dynamics and ensure optimal operating conditions.

2.3. Experimental protocol

The experiments were designed to optimise the operating conditions of the MC-AnPBR system, with the aim of maximising the separation of a gaseous VFAs stream from the feed solution in the MC and their transfer to the AnPBR, enhancing the growth of PNSB, with a focus on monitoring the long-term effects of VFAs transfer on PNSB performance and system stability. The key parameter in optimizing these outcomes was the applied OLR ($OLR_{applied}$) of gaseous VFA stream impacting both VFA transfer and PNSB biomass production. The OLR was optimized by changing temperature and total contact time ($t_{c,tot}$) of the MC system as critical parameters influencing VFA gas transfer (Lo Coco et al., 2024; Yesil et al., 2021). The configuration and operating conditions of the AnPBR were maintained unchanged in all experimental runs (see supporting material). Table 1 provides an overview of the experimental periods aimed at optimizing the process, along with the corresponding operating parameters of the MC system. Preliminary experiments were conducted at four different total contact times in the MC (i.e. 0.96, 1.92, 2.88, and 4.32 min) at room temperature to establish a baseline (Preliminary Test, 1–9 days, Table 1). Following these preliminary experiments, the MC-AnBPR was operated for 12 days at a MC total contact time of 1.92 min to achieve an applied OLR ($OLR_{applied}$) of 0.7 ± 0.2 g $COD{\cdot}L^{-1}{\cdot}d^{-1}$ under controlled temperature of 20 ± 1°C (Period 1, Table 1). Then the OLR was increased to 1.3 ± 0.3 g $COD{\cdot}L^{-1}{\cdot}d^{-1}$ in Period 2 by increasing the MC total contact time ($t_{c,tot}$) to an optimal of 2.88 min at 20 ± 1°C observed in Preliminary test (Table 1). In Periods 3 and 4, the OLR was increased by changing the MC temperature to 25 ± 1°C and 32 ± 1°C, respectively, to investigate the effect of temperature and the effect of different OLR on the biomass growth in the AnPBR. Period 4 (64–160 days) was initially designed as a single operating stage. However, due to experimental observations of instability in pH levels and their effect on PNSB growth and adjustment of operating conditions, this period was subsequently divided into two sub-periods: Period 4.1 (64–76 days), characterised by unstable conditions under higher OLR (5.8 ± 0.6 $gCOD{\cdot}L^{-1}{\cdot}d^{-1}$ under 2.88 min of contact time and 32 ± 1°C of feed temperature); and Period 4.2 (78–160 days), where OLR was reduced to 3.9 ± 0.8 $gCOD{\cdot}L^{-1}{\cdot}d^{-1}$ by reducing contact time from 2.88 to 1.92 min, allowing the system to reach long-term stability.

2.4. Measurement and analysis

2.4.1. Methodology and performance assesment

The performance of VFA transfer in gaseous phase in the MC was evaluated in terms of VFA mass flux (j), applied OLR ($OLR_{applied}$) and transfer efficiency (η).

Mass flux (j, $g{\bullet}m^{-2}{\cdot}h^{-1}$) of the VFA (i) through the membrane studied by a mass balance approach was calculated as:

$$j_i = \frac{m_{i,t}}{A \bullet t} = \frac{\left([VFAs]_{F,t_0} - [VFAs]_{F,t}\right) \bullet V_{feed}}{A \bullet t} \quad (1)$$

where $m_{i,t}$ is the mass of a VFA (*i*) transferred across the membrane with a surface area A (m^2) at time *t* (h^{-1} or d^{-1}).

The mass transferred ($m_{i,t}$) for a given VFA *(i)* is calculated as the difference between the initial mass ($[VFAs]_{F,t_0}$) present in the volume liquid phase at t_0 and the remaining mass ($[VFAs]_{F,t}$) at a specific time (*t*), representing the net transfer across the membrane over the duration of the process and a performance indicator during experimental run.

To describe the kinetics of the transfer more accurately, the overall mass transfer coefficient (K_e) was introduced into the mathematical formulation, which takes into account the concentration decay over time according to first order kinetics (Eq. (2)):

$$ln\frac{[VFAs]F,t_0}{[VFAs]F,t} = -Ke\frac{A}{V_{feed}}t \quad (2)$$

This equation shows how the change in VFAs concentration ($ln\frac{[VFAs]F,t_0}{[VFAs]F,t}$) over time (t) is a function of the mass transfer coefficient (K_e), membrane surface area (A) and volume of the feed solution (V_{feed})

By integrating this equation with the initial mass balance (Eq. (1), the flux of the VFA over time can be calculated by the following equation:

$$j_i = \frac{[VFAs]F,t_0 \bullet V_{feed,t_0}}{At}\left(1 - e^{\frac{K_e At}{V_{feed}}}\right) \quad (3)$$

This equation indicates that the amount of VFA transferred through the membrane surface area over time depends by the transfer coefficient k_e and the inital VFA mass.

The applied organic loading rate (OLR, $gCOD{\bullet}L^{-1}{\cdot}d^{-1}$) is the mass rate of organic substrate ($gCOD_{VFA}$) provided per unit volume of bioreactor. OLR was calculated as:

$$OLR_{applied} = \frac{j \times A}{V_{reactor}} = \frac{[VFAs]F,t_0 \bullet V_{feed,t_0}}{V_{reactor}}\left(1 - e^{\frac{K_e At}{V_{feed}}}\right) \quad (4)$$

where $j_{i,d} \times A$ represent the mass of a VFA (*i*) transferred across the membrane each day (d) and additional to volume of reactor ($V_{reactor}$). This relationship allows the transfer of VFA to be described as a function

of operating parameters and membrane properties, providing a quantitative reference to assess the effect of recovery on the stability of the biological system and process conditions.

The VFA transfer efficiency (η, %) was calculated as:

$$\eta = \frac{VFA_{trasfered}}{VFA, t_0} * 100 \quad (5)$$

where VFA transferred are the VFA transfer across the MC and VFA,t_0 are the VFAs at initial time.

To optimize the conditions for an effective VFA mass transfer in the MC, it was considered the contact time of a single feed cycle through the MC ($t_{c,cycle}$, s) by Eq (6):

$$t_{c,\,cycle} = \frac{V_{MC}}{Q} \quad (6)$$

where V_{MC} (mL) is the volume of the MC lumen and Q (mL·min^{-1}) is the flow rate of the feed solution.

Then the number of cycles (n° cycle) that the feed volume (V_{feed}) recirculates through the MC at a specific flow rate (Q) during the stripping time (t) of each experimental run was calculated according to Eq. (7):

$$n^{\circ}\,cycle = Q \bullet \frac{t}{V_{feed}} \quad (7)$$

The stripping time (t) coincides with the actual duration of the phases where the VFA mass transfer occurred through the MC.

By the combination of Eq (4) and Eq (5), it was calculated the total contact time $t_{c,tot}$ (min, Eq. (8) which represents the total time that the V_{feed} and the MC were in contact along the stripping time (t):

$$tc, tot = t_{c,cycle} \times n^{\circ} cycle \quad (8)$$

The reactor active biomass was defined by subtracting the gMLVSS•L^{-1} and the amount of gPHA•L^{-1} (see section 2.7.4), in order to determine the concentration of non-polymeric biomass, or active biomass ($gx_{PB,\,MLVSS}$•L^{-1}).

The performance of the photobioreactor was assessed by calculating the biomass production rate (P_{obs}, gX·L^{-1}·d^{-1}) and the observed yield (Y_{obs}, gX·gCOD^{-1}).

The active biomass production rate was calculated from the concentration of the active biomass produced (X, gMLVSS·L^{-1}) from flow rate (Q) for the hydraulic retention time (HRT) set for the photo-anaerobic bioreactor:

$$P_{X,PB} = \frac{Q \bullet [X]_{PB.MLVSS}}{HRT} \quad (9)$$

$$Y_{obs} = \frac{X_{PB.COD\,(produced)}}{COD_{VFAs\,(consumed)}} = \frac{Q \bullet [X]_{PB.MLVSS}}{\left[[VFAs]F, t_0 \bullet V_{feed,t_0}\left(1 - e^{\frac{K_e A}{V_{feed}}t}\right)\cdot E\right]} \quad (10)$$

The biomass observed yield takes into account the actual biomass production measured for the reactor and the substrate removed as COD. The biomass produced (X) was calculated as COD equivalent of biomass, considering the theoretical ratio of 1.75 gCOD·gVSS^{-1} (Allegue et al., 2022). While, the COD consumed (COD_{VFA} – $COD_{effluent}$) was calculated as $gCOD_{VFA}$ consumed (j •A) until the duration of the reaction phase transferred via gas by using MC under different operating membrane conditions and converted into different COD forms (active biomass, hydrogen and COD present in the supernatant effluent). By considering the substrate removal efficiency defined as $\eta = COD_{VFA} - \frac{COD_{effluent}}{COD_{VFA}}$, it was expressed the effluent mass ($COD_{effluent}$) in term of the efficiency E. All experiments were performed in triplicate. Results are reported as mean values ± standard deviation (SD). Uncertainty in calculated parameters (e.g. mass fluxes, yields and productivities) was determined by error propagation using the standard deviations of the measured variables.

2.4.2. Analytical methods

Routine parameters such as chemical oxygen demand (COD), mixed liquor volatile suspended solids (MLVSS), were measured according to the standard methods (APHA, 1998; IRSA-CNR, 2003 ISBN 88–448-0083–7). VFAs concentrations were monitored at the inlet and outlet of feed solutions using an ICS 1100 ion chromatograph from Thermo Fisher Scientific, according to the method described by (Righetti et al.,2020). PO_4^{3-} – P concentration was measured into bioreactor using Dionex ICS-900 with AG14 column and AMMS 300 suppressor on filtered samples (0.2 μm, Whatman syringe filters). Electrical conductivity (mS·cm^{-1}), pH, oxidation–reduction potential ORP (mV), temperature (°C) and O_2 dissolved (mgO_2·L^{-1}) were measured using multiparameter probe (HI9829 Hanna Instrument) during each phase of bioreactor condition (see section 2.4.2) and in the inlet and outlet of feed. Headspace composition was determined by Micro GC Fusion® Gas Analyzer by sampling directly from the bioreactor. Analytic grade acetic acid (HAc, $C_2H_4O_2$), propionic acid (HPr, $C_3H_6O_2$), butyric acid (HBu, $C_4H_8O_2$), and caproic acid (HCa, $C_6H_{12}O_2$) from Sigma-Aldrich (Italy) were used for the feed solution. Sodium hydroxide (NaOH, ACS reagent ≥ 97.0 % purity, pellets) and sulphuric acid (H_2SO_4, ACS reagent 95.0–98.0 %) used for pH adjustment were purchased from Sigma-Aldrich (Italy). Disodium succinate ($C_4H_4Na_2O_4$, Sigma-Aldrich reagent ≥ 99.0 %), Ammonium acetate ($C_2H_7NO_2$, ACS reagent ≥ 98.0 %), Iron(III)-citrate ($C_6H_5FeO_7$, Sigma-Aldrich reagent ≥ 98.0 %), yeast extract (YE, ACS reagent), Potassium dihydrogen phosphate (KH_2PO_4, ACS reagent 99 % purity), Magnesium Sulphate Heptahydrate ($MgSO_4$·$7H_2O$, ACS reagent ≥ 99.0 % purity), Sodium Chloride (NaCl, Sigma-Aldrich reagent ≥ 99.5 % purity), Ammonium Chloride (NH_4Cl, Sigma-Aldrich reagent ≥ 99.5 % purity), Calcium chloride dihydrate ($CaCl_2$·$2H_2O$, ACS reagent ≥ 99.0 %) and L-Cysteiniumchloride (ACS ≥ 98.0 %), Vitamin B_{12} (ACS, 98+%) were used as components of the nutrient solution and the modified medium for *Rhodospirillaceae (German Collection of Microorganisms and cell cultures GmbH_DSMZ: https://www.dsmz.de)* for the preparation of the inoculum. Zinc sulfate heptahydrate ($ZnSO_4$·$7H_2O$, Sigma-Aldrich reagent ≥ 99.0 %), Manganese(II) chloride tetrahydrate ($MnCl_2$·$4H_2O$, ACS reagent ≥ 98.0 %), Boric acid (H_3BO_3, ACS ≥ 99.5 %), Cobalt(II) chloride hexahydrate ($CoCl_2$·$6H_2O$, Sigma-Aldrich reagent ≥ 98.0 %), Copper(II) chloride dihydrate ($CuCl_2$·$2H_2O$, ACS ≥ 99.0 %), Nickel(II) chloride hexahydrate ($NiCl_2$·$6H_2O$, ACS reagent ≥ 98.0 %) and Sodium Molybdate Dihydrate (Na_2MoO_4·$2H_2O$ ACS reagent ≥ 99.0 %), were used as constituents of the trace element solution used for the preparation of the culture medium and nutrient solution.

2.4.3. Microbial community analysis

To analyse the microbial community composition in the AnPBR, 2 mL of the biomass was centrifuged at 3000 rpm for 2 min. The resulting bacterial pellet was then sent to BMR Genomics for 16S rRNA gene amplicon sequencing analysis, following the protocol detailed by BMR Genomics. DNA was extracted from the bacterial pellet using the DNeasy® 96 PowerSoil® Pro QIAcube® HT Kit (Qiagen) and subsequently purified with the QIAcube Kit (Qiagen). The V4 gene region was amplified by PCR using universal primers for bacteria and archaea (Takahashi et al., 2014). Then, the DNA was purified with the Thermolabile Exonuclease I (NEB). Nextera XT DNA Library Preparation kit (Illumina) was used to prepare the library, which was normalised, multiplexed, and sequenced on an Illumina MiSeq. Quality evaluation was performed using the PASTQC software, and taxonomic analysis was performed using a QIIME2 pipeline and Greengenes 8_13, Silva 132, and RDP databases. The change in the microbial community was represented as the relative abundance of each family compared to the total number of families present in the sample.

2.4.4. Biomass characterization

The nutritional value, the crude protein amount and the total and the essential amino acids (EAA) were measured from the biomass obtained from the PNSB-bioreactor. The amount of crude protein was determined from the nitrogen content, which was determined using the Kjeldahl method and multiplied by the conversion factor 6.25 (IRSA-CNR). Total nitrogen in the bioreactor was measured using the Kjeldahl method according to standard method (APHA, 1998; IRSA-CNR, 2003). The essential amino acid (EAA) composition before oxidation and hydrolyzation of the samples was determined in triplicate by ion chromatography with post-column derivatization using ninhydrin according to the method (IRSA-CNR). Cysteic acid was used as an indicator to measure the combined amounts of cystine and cysteine, with the total reported as "cysteine.". Methionine was determined as methionine sulfone and then expressed ad "methionine". Tryptophan was measured as described in the AOAC method 2017.03. The measured protein content in the biomass and the EAA composition of the protein were used to determine the chemical score (CS) (Pesante et al.,2024). This index was used to assess the nutritional quality of the PNSB proteins in the context of their potential application as fish feed. The CS indicates how well a protein meets the EAA requirements of an animal. The CS of an EAA was determined as the amount of the EAA measured in the microbial PNSB protein relative to the amount of that EAA in a reference protein. The reference proteins were Chinook salmon (Pesante et al.,2024) Tilapia (*Oreochromis mossambicus* sp., *Oreochromis niloticus* sp. (Pesante et al.,2024) and commercial feed for fishmeal (Delamare-Debouteville et al., 2019).

$$\text{Chemical score (CS)} = \frac{\%\ of\ a\ given\ EAA\ in\ SCP\ protein}{\%\ \text{of the same EAA in reference protein}} \text{x100} \quad (11)$$

The SCP quality parameter was calculated to quantify the proportion of biomass composed of bioproducts with significant nutritional and functional value, contributing to its potential as a source of SCP. This parameter is expressed as gBioP•gMLVSS^{-1} and is defined as the sum of the biomass fractions corresponding to crude protein (CP), pigments (BChl and Crts) and polyhydroxyalkanoates (PHAs). The percentage of SCP quality reflects the sum of these components relative to the total biomass (MLVSS) and provides a comprehensive metric for assessing the quality of biomass as a potential feedstock for SCP applications. This parameter serves as a key indicator of the system's ability to produce high quality biomass under different operating conditions.

2.4.5. PHA analysis

The analysis of the PHA content in the PNSB biomass was conducted by gas chromatograph (GC) following the method by (Braunegg et al., 1978). 10 mg of the freeze-dried pellets were finely ground and dissolved in 1 ml of chloroform, 2 ml of methanol containing 3 % (v/v) sulfuric acid and 1 ml of a 0.5 % (w/v) benzoic acid solution in chloroform. The samples were then heated at 100 °C for 4 h, after which 1 ml of distilled water was added, and the solution was mixed for 15 min and then centrifuged at 2100 rpm for 2 min. The resulting pellet (organic phase) was separated and analysed by GC (Braunegg et al., 1978). Standards for the calibration curve were prepared with pure poly(3-hydroxybutyric acid-*co*-3-hydroxyvaleric acid) (Sigma, 403105) and treated following the same protocol. PHA content in the experimental samples was calculated as the percentage of the measured PHA mass (g) relative to the total organic biomass of the samples, expressed as the volatile suspended solids (VSS, g). Also, the PHA concentration was converted into COD units following the oxidation stoichiometry: 1.67 mg of O_2•mg of PHB^{-1}, 1.92 mg of O_2•mg of PHV^{-1} (Frison et al., 2015) in order to define the PHA storage yield ($Y_{PHA/VFA}$, g of COD_{PHA}•g of COD_{VFA}^{-1}).

2.4.6. Pigment analysis

50 ml of the culture was centrifuged for 15 min at 10,000 g and the supernatant was discharged. The cells were resuspended 8 ml of acetone 80 % with Na_2CO_3 (buffered at slight alkaline pH to avoid BChl degradation by loss of the chelated Mg^{2+}) and lysed with glass beads (Precellys Evolution, Bertin) in order to extract the pigments in according to (Cazzaniga et al., 2022; Chazaux et al., 2022). It should be noted that, unlike the approach taken by (Grassino et al., 2022), the method used in this study is not primarily intended for the precise quantification of individual carotenoids but rather for determining the total carotenoids and Bchl content by spectrophotometric analysis. Extract samples were centrifuged at 12000 rpm for 10 min at 4 °C to eliminate cell debris. Absorption spectra of supernatants were measured in the 350–900 nm range (Jasco UV3000); Bchl and carotenoids concentration was determined by absorption spectra using extinction coefficients (see supporting material) corrected for overlapping bands (Chazaux et al., 2022). The quantification of total pigment content in PNSB biomass was derived from the analysis of acetone-extracted pigment spectra. The spectra show characteristic absorption peaks for bacteriochlorophyll (BChl) and carotenoids (Crts), with BChl showing pronounced absorption at 350 nm and in the Q_x (~580 nm) and Q_y (~770 nm) bands and the Crts showing a peak ~ 475 nm.

3. Results and discussion

The potential to continuously produce protein-rich biomass in an AnPBR on a gaseous stream of VFAs recovered from fermented broth via MC, preventing direct contact between the fermented broth and the biomass, was investigated. Over an experimental period of 160 days, divided into four different periods: Period 1 (*P*1, 11–23 days), Period 2 (*P*2, 28–43 days), Period 3 (*P*3, 44–63 days) and Period 4 (*P*4, 64–160 days, divided in subperiod 4.1 and 4.2), each representing specific operating conditions and system performance assessments. The extended duration of 160 days, particularly the consistent performance observed in Period 4.2 (over multiple HRTs with less than 5 % variation in biomass and pH), demonstrated the long-term reliability and scalability of the MC–AnPBR system. The operating conditions of the MC were varied to evaluate the effects of OLR on the PNSB production in the AnPBR.

3.1. Reactor system optimization

3.1.1. Preliminary tests

Preliminary tests were conducted to assess the impact of different experimental run durations (stripping time (t_{strip})) in the MC on VFA transfer efficiency and thus the OLR to the bioreactor, with the aim of selecting the run duration for the subsequent experimental phases that provides a balance between VFA mass transfer and operating efficiency of the overall MC-AnPBR system.

Four stripping times were tested: 2, 4, 6, and 9 h, corresponding to total contact times ($t_{c,tot}$) of 0.96, 1.92, 2.88, and 4.32 min, respectively, under room temperature conditions and a vacuum of 100 mbar (Table 1). At the initial acidic pH of the synthetic solution (3.0 ± 0.1), over 90 % of the acids are in their protonated form calculated using the equation $[HA]_i = [A]_i \left(\frac{10^{-pH}}{10^{-pH}+10^{-pKa}}\right)$, which increases the partial pressure and diffusion velocity of VFAs increase, thereby enhancing their transfer through the MC (Lo Coco et al., 2024).

However, a negligible mass transfer of HAc was observed at striping time of 2 h, but it increased significantly when the stripping time was extended to 4 h. The longer stripping time resulted in higher diffusion and transfer of HAc across membrane which led to higher OLR applied (Table 2) (Kaya and Hasanoğlu, 2022; Lo Coco et al., 2024). In contrast, the mass transfer of HBu and HPr did not change significantly with increasing $t_{c,tot}$, while their transfer rate (mass flux, j) decreased at longer stripping (Table 2). This phenomenon is probably due to the vacuum-driven pressure gradient, which facilitates rapid stripping of

Table 2
Transfer efficiency (η %), Flux (gCOD·m^{-2}h^{-1}) and mass transfer (gCOD) for each acid during the preliminary test under different stripping ($t_{stripp.}$) time and total contact time ($t_{c,tot}$).

		VFAs			Acetic acid (HAc)			Propionic acid (HPr)			Butyric acid (HBut)		
t_{strip} (h)	$t_{c,tot}$ (min)	η (%)	j (g_{COD}·m^{-2}h^{-1})	Mass transfer (g_{COD})	η (%)	j (g_{COD}·m^{-2}h^{-1})	Mass transfer (g_{COD})	η (%)	j (g_{COD}·m^{-2}h^{-1})	Mass transfer (g_{COD})	η (%)	j (g_{COD}m^{-2}h^{-1})	Mass transfer (g_{COD})
2	*0.96*	2 ± 1	1.0 ± 0.06	0.4 ± 0.03	3 ± 1	0.65 ± 0.04	0.3 ± 0.02	5 ± 1	0.30 ± 0.01	0.10 ± 0.01	0	0	0
4	*1.92*	7 ± 1	2.4 ± 0.2	2.1 ± 0.2	6 ± 2	1.5 ± 0.4	1.3 ± 0.4	9 ± 1	0.62 ± 0.1	0.5 ± 0.1	9 ± 2	0.30 ± 0.1	0.30 ± 0.01
6	*2.88*	9 ± 1	2.2 ± 0.2	2.9 ± 0.3	10 ± 2	1.7 ± 0.3	2.3 ± 0.4	7 ± 1	0.34 ± 0.1	0.5 ± 0.1	5 ± 1	0.10 ± 0.01	0.10 ± 0.01
9	*4.32*	14 ± 3	1.8 ± 0.2	3.6 ± 0.4	18 ± 4	1.6 ± 0.22	3.2 ± 0.4	5 ± 1	0.14 ± 0.02	0.3 ± 0.1	5 ± 2	0.1 ± 0.02	0.10 ± 0.01

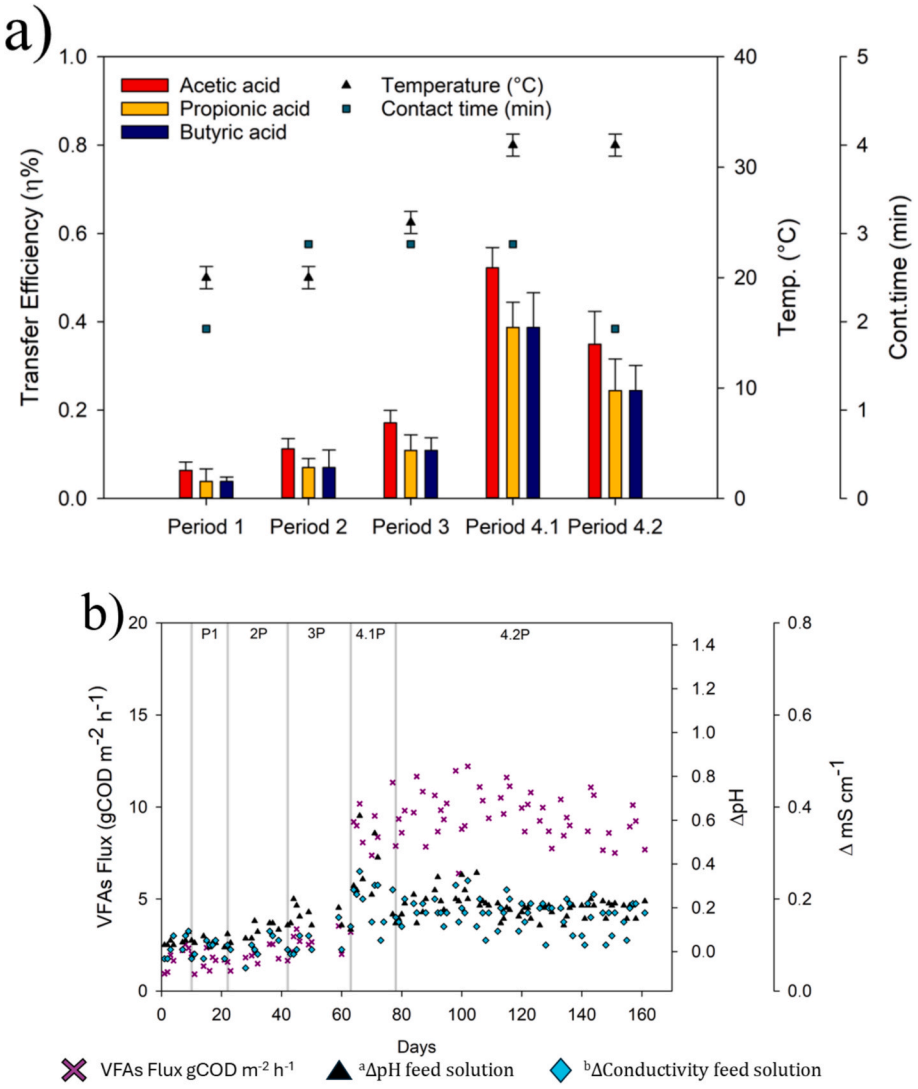

Fig. 2. a) Transfer efficiency (η%) of acetic, propionic and butyric acids in the MC under different operating conditions, i.e. temperature and total contact time. The error bars represent the standard deviation of the transfer efficiency measurements for each acid in each period. b) Temporal dynamics of VFAs flux, ΔpH and Δconductivity during the operating period in the feed tank. [a]Δ = $pH_{post\text{-}stripping}$ – $pH_{pre\text{-}stripping}$; [b]Δ= Cond. $_{pre\text{-}stripping}$ – Cond.post-$_{stripping}$ c) Temporal dynamics of OLR (gCOD•L^{-1}•d^{-1}), biomass (gX_{active} •L^{-1}) and pH reactor in the effluent. d) Trends in biomass production (kgX·m^{-3}·d^{-1}), crude protein production (kgCP·m^{-3}·d^{-1}), and percentage of crude protein (% Crude Prot.) across the experimental periods (Period 2 to Period 4).

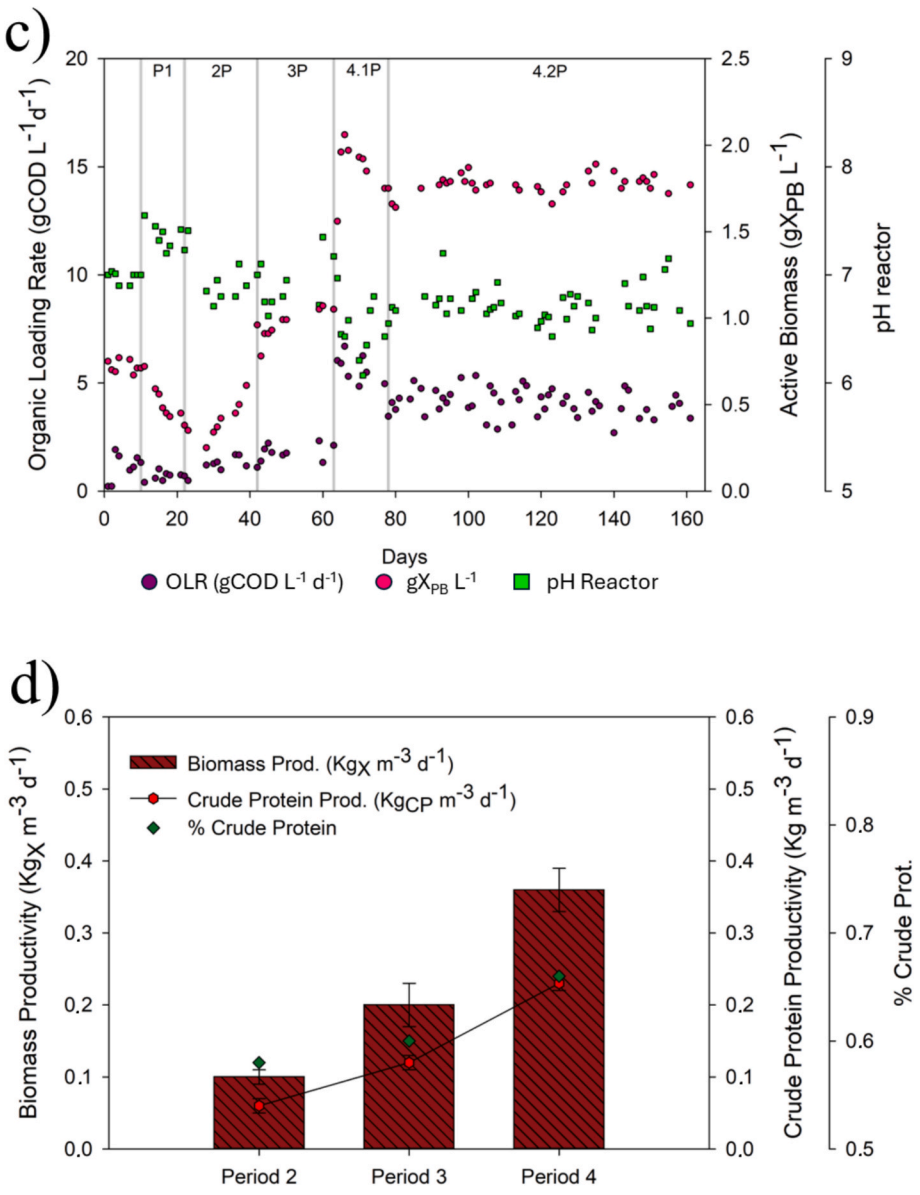

Fig. 2. (*continued*).

HBu and HPr from the liquid phase, causing the system to approach partial pressure equilibrium. Once the equilibrium is established, the driving force for further transfer diminishes, effectively limiting further recovery regardless of the length of the experiment.

At the same time, the longer operational duration allowed more HAc to be transferred, increasing its total mass transfer (Table 2). Therefore, the $t_{c,tot}$ of 1.92 min corresponding to the stripping duration of 4 h was selected as it was enough to achieve the target OLR applied to the AnPBR by the VFA transferred through the MC.

In parallel to the preliminary tests with the MC system, the AnPBR was started-up. As shown in figure 2(c), the initial concentration in terms of mixed liquor volatile suspended solids in the AnPBR inoculated with *R. palustris* sp. (*Section 2.2.1*) was 0.75 ± 0.08 gMLVSS·L^{-1} (corresponding to a production rate 0.14 ± 0.01 gMLVSS·L^{-1}·d^{-1}). During this initial AnPBR operation test (1–10 days), the average biomass production rate was 0.14 ± 0.01gMLVSS·L^{-1}·d^{-1}. The anaerobic condition was confirmed by the absence of dissolved oxygen (mgO_2·L^{-1}) in the mixed liquor during the reaction phase.

3.1.2. Experimental period 1

During Period 1, the reactor did not stabilise, with biomass production decreasing from 0.14 to 0.07 g MLVSS L^{-1} d^{-1}. This was due to a loss of anaerobic conditions caused by a leak, which reduced vacuum pressure and lowered VFA transfer efficiency, allowing oxygen to enter the system. Furthermore, the transfer performance of VFAs in terms of flux were not consistent with preliminary tests. The flux (j) of VFAs was 40 % lower than preliminary data (Table 2; see also the initial section of Fig. 2b, days 0–10), particularly for acetic, propionic and butyric acid, which were 1.2 ± 0.4, 0.08 ± 0.02 and 0.2 ± 0.05 gCOD·m^{-2}·h^{-1}, respectively. The 40 % lower VFA flux compared to the preliminary tests was primarily due to the loss of vacuum in the MC (i.e., a reduced driving force for gas transfer). In parallel, oxygen intrusion (ORP + 185 mV, DO ~ 1 mg O_2·L^{-1}) mainly affected the biology, inhibiting photoheterotrophic PNSB growth. This effect is consistent with previous studies showing that, in the presence of oxygen, PNSBs exhibit lower growth rates around 2.4 gVSS·$gVSS^{-1}$·d^{-1} at 32–36 °C than aerobic heterotrophic bacteria 6.0 gVSS·$gVSS^{-1}$·d^{-1} at 20 °C (Metcalf & Eddy, 2013) (Capson-Tojo et al., 2021).

3.1.3. Experimental period 2

In Period 2, the MC system was operated at a total contact time of 2.88 min and a stripping time of 6 h, under a controlled temperature of 20 ± 1 °C (Table 1). Under these conditions, the transfer efficiencies of HAc (C2), HPr (C3) and HBu (C4) were 11 ± 1 %, 7 ± 2 % and 7 ± 2 %, respectively (Fig. 2 (a)), Resulting in an OLR of 1.3 ± 0.4 $gCOD{\cdot}L^{-1}{\cdot}d^{-1}$, corresponding to a mass transfer of 2.6 ± 0.4 gCOD, an increase of 44 % compared to Period 1. The total VFA flux was 1.99 ± 0.37 $gCOD{\cdot}m^{-2}{\cdot}h^{-1}$, higher than in Period 1 according to 1.55 ± 0.28, 0.14 ± 0.04 and 0.30 ± 0.11 $gCOD{\cdot}m^{-2}{\cdot}h^{-1}$ for HAc, HBu and HPr, respectively. These values fall within the lower range reported in the literature for typical VFA fluxes, which vary between ~ 1 and 5 $gCOD{\cdot}m^{-2}{\cdot}h^{-1}$ depending on the feed concentration, membrane type, and operating mode (Aydin et al., 2018; Tugtas, 2014; Yesil et al., 2021). Yesil et al., for instance, reported an HAc flux of 4.9 $gCOD{\cdot}m^{-2}{\cdot}h^{-1}$ using a 2 $g{\cdot}L^{-1}$ solution and a smaller membrane surface area (0.0012 m^2) at 21 °C. The lower fluxes observed in this study can be attributed to differences in membrane configuration (surface area of 0.22 m^2) and the higher COD concentration of the synthetic mixture.

The AnPBR was reinoculated as the low relative abundance of PNSB in the reactor resulted from the non-sterile and unfavourable conditions of Period 1. At the beginning of the Period 2, the AnPBR was reinoculated with the same type of PNSB inoculum used in Period 1 up to obtain an initial concentration of 0.30 ± 0.02 $gMLVSS{\cdot}L^{-1}$ in order to get a faster response from the increased flux in VFA on PNSB production rate.

The pH in the bioreactor was maintained stable at 6.91 ± 0.14 during the overall Period 2 (Fig. 2 (c)), which is within the optimal levels for microbial growth, lower than Period 1 (7.36 ± 0.11) (Sepúlveda-Muñoz et al., 2020). Particularly, Fig. 2 (c) shows that when the applied OLR was increased to 1.3 ± 0.4 $gCOD{\cdot}L^{-1}{\cdot}d^{-1}$, the average pH in the AnPBR drops at 6.91 ± 0.14 accordingly during the discharge phase (effluent). The reactor pH was most affected during the VFA loading (stripping) phase, reaching 6.83 ± 0.14 due to the direct transfer of VFAs into the system, which also caused variations in pH and conductivity (0.11 and 0.17 $mS{\cdot}cm^{-1}$, respectively ΔpH and Δconductivity) in the feed solution (Fig. 2 (b)). VFA uptake by PNSB then resulted in a pH alkalization leading to an increase of the value up to 6.91 ± 0.14 in the effluent phase.

During this period, the total VFAs removal efficiency was 85 %, with 98.5 % of the removed VFAs being converted into PHA, H_2 and active biomass, as described in the following section. In particular, the PNSB biomass production rate was 0.16 ± 0.05 $gX_{PB}{\cdot}L^{-1}{\cdot}d^{-1}$ (0.17 ± 0.05 $gMLVSS{\cdot}L^{-1}{\cdot}d^{-1}$) under photoheterotrophic growth, which resulted in an observed biomass yield (Y_{obs}) of 0.32 ± 0.01 $gCOD{\cdot}gCOD^{-1}$, derived from a growth of $\Delta X_{COD} = 0.44 \pm 0.07\ gCOD{\cdot}d^{-1}$.

Allegue et al., 2022 reported a higher rate of 0.42 $gVSS{\bullet}L^{-1}{\bullet}d^{-1}$ in an MPBR treating the effluent from organic fraction of municipal solid waste (OFMSW) digesters under similar OLR conditions (1 $gCOD{\bullet}L^{-1}{\bullet}d^{-1}$). This discrepancy could be attributed to their lower SRT of 4 days, as shorter SRTs typically increase production rates. However, processes such as OFMSW fermentation often result in the accumulation of non-biodegradable COD (nbCOD) in the mixed liquor, which contributes to non-biodegradable volatile suspended solids (nbVSS) and inert non-volatile solids (iTSS). These solids reduce process efficiency and degrade the quality of the final biomass (Metcalf & Eddy, 2013). In contrast, the growth of PNSB biomass using VFAs supplied in gaseous form enhances its purity, as it prevents the contamination of the culture with any non-biodegradable VSS potentially.

The crude protein content of the produced biomass reached 58 % based on dry mass, aligning with the typical values observed in PNSB mixed cultures (450–650 $g{\cdot}Kg^{-1}$) (Capson-Tojo et al., 2020b), which resulted to a crude protein production of 0.06 ± 0.01 $kgCP{\bullet}m^{-3}{\bullet}d^{-1}$ (Fig. 2 (d)). Biomass grown on gaseous VFA provided a higher protein content per unit of VSS due to the absence of non-biodegradable VSS typically present in the fermentation liquid, improving the quality of SCP.

Anaerobic conditions were maintained in the reactor, as evidenced by the absence of dissolved oxygen in the mixed liquor, and by the gas composition measured in the bioreactor's headspace with 98.5 % of N_2, 1.4 % of CO_2, 0.004 % of H_2, and < 0.1 % oxygen. The absence of oxygen was also confirmed by the negative ORP values recorded during all three operational phases of the bioreactor, indicating constant reducing conditions that favoured photoheterotrophic metabolism (McKinlay and Harwood, 2011). The lowest ORP of −75 mV was observed during the carbon loading (stripping phase). The presence of hydrogen in the headspace gas composition represent a product coming from the nitrogenase reaction. The N_2-rich environment stimulates the hydrogen production, affecting the Calvin cycle flux, essential for the photoheterotrophic growth (McKinlay and Harwood, 2011).

The low ORP values measured in the AnPBR support the accumulation of PHA as an electron sink (Bond-Watts et al., 2011). In fact, 0.12 g PHA•g dry $mass^{-1}$ was measured in the produced biomass, corresponding to a PHA storage yield of 0.22 $gCOD_{PHA}{\bullet}gCOD_{VFA}^{-1}$ derived from a COD_{VFA} consumed of 74 %. A peak PHA content of 0.18 g PHA•g dry $mass^{-1}$ and a HB/HV ratio of 2.6 was observed at the end of the stripping phase. These values for PHA content are consistent with those reported by (Capson-Tojo et al., 2020b), particularly for those using a VFA mixture as a carbon source (40–190 $g{\cdot}kg^{-1}$). The results reflects the correlation of the PHA composition on the substrate used, where HPr was present at 10 % of the VFA influent of the AnPBR. The results reflect the correlation of PHA composition with the substrate used, where HPr was present at 10 % of the VFAs fed into the AnPBR, which generally acts as a precursor in PHV synthesis (Huang et al., 2025).

3.1.4. Experimental period 3

In Period 3, the applied OLR to the AnPBR was increased to 1.9 ± 0.4 $gCOD{\cdot}L^{-1}{\cdot}d^{-1}$ (Fig. 2 (c)) by raising the temperature of the VFA-feed solution up to 25 ± 1°C. This temperature enhanced VFA mass transfer, and its effect on AnPBR performance was studied, with particularly regard to the PNSB production rate and protein productivity.

The transfer efficiency of HAc and HPr in the MC improved to 17 ± 2 % and 11 ± 3 %, respectively, while that of HBu slightly decreased to 3 %. Similarly, the mass transfer rate increased to 2.51 ± 0.40 $gCOD{\cdot}m^{-2}{\cdot}h^{-1}$ (Fig. 2 (b)) for HAc and to 0.23 ± 0.08 $gCOD{\cdot}m^{-2}{\cdot}h^{-1}$ for HPr, while decreasing to 0.13 ± 0.03 $gCOD{\cdot}m^{-2}{\cdot}h^{-1}$ for HBu. The improved transfer observed for HAc and HPr was consistent with their chemical properties, such as the smaller molecular size and higher volatility that make them more responsive to increased temperature compared to HBu, supporting to data of ΔpH and Δconductivity in the feed tank (figure 2 (b)).

As evidenced by the VFA mass transfer, an abundant supply of VFAs is crucial for supporting PNSB growth and protein synthesis. However, excessively high residual concentrations of VFAs in the mixed liquor can disrupt the stability of the AnPBR, posing challenges in maintaining consistent bioreactor conditions, particularly with respect to pH stability during the stripping phase.

As shown in Fig. 2 (c), the increased of the VFA transfer led to a decrease of the pH to 6.74 ± 0.12 at the end of the stripping phase of the AnPBR, while raised to 6.89 ± 0.25 in the discharge phase. Compared to Period 2, in this period the OLR was 45 % higher leading to an increase of the concentration of the biomass in the AnPBR from 0.78 ± 0.09 $gX_{PB}{\cdot}L^{-1}$ (Period 2) to 1.06 ± 0.04 $gX_{PB}{\cdot}L^{-1}$ (Period 3).

Although the increase in OLR allowed for higher concentrations of active biomass in the AnPBR and it consequently boosted system's production rates to 0.21 ± 0.01 $gX_{PB}{\cdot}L^{-1}{\cdot}d^{-1}$. This positive correlation between OLR and biomass production rate has been reported in the literature (Liu et al., 2016), in particular they observed that doubling the OLR resulted in approximately a two-fold increase in the biomass production rate. While, it was observed a 35 % increase in the biomass production rate with a 45 % increase in OLR compared to Period 2. The observed growth rate stabilized at 0.31 ± 0.02 $gCOD{\cdot}gCOD^{-1}$, comparable to the values recorded during the Period 2 (Fig. 4).

The biomass obtained in Period 3 accounted for a percentage of CP of 60 % based on dry mass, slightly higher compared to Period 2, which led to an overall crude protein productivity of 0.12 ± 0.01 $kgCP \cdot m^{-3} \cdot d^{-1}$ doubled compared to the previous period (Fig. 2 (d)). The protein content obtained in the Period 2 and 3 are in line with typical values observed in the literature, representing about an average content characterizing PNSB (Hülsen et al., 2022a).

During the operation, anaerobic conditions were maintained throughout AnPBR operation, with a dissolved oxygen content in the mixing liquor below 0.5 % and 95.1 % N_2, 4.4 % CO_2 and 0.009 % H_2 measured in the bioreactor headspace.

In Period 3, a PHA content of 0.09 g PHA•$g^{-1}_{dry\ mass}$ a HB/HV ratio of 2.4 was measured in the AnPBR discharge phase. This supports the hypothesis of (Allegue et al., 2022), that elevated OLR conditions may influence negatively the PHA production efficiency, shifting the metabolic balance away from optimal PHA accumulation.

3.1.5. Experimental period 4

At the beginning of Period 4, the feed temperature was increased to 32 ± 1°C to enhance VFA transfer through the MC system, with the aim of achieving a higher OLR in the AnPBR and investigating its effects on biomass growth and composition. As a result of the temperature increases, the total VFA mass flux reached 8.81 ± 2.17 $gCOD \bullet m^{-2} \bullet h^{-1}$, resulting in an applied OLR of 5.8 ± 0.6 $gCOD \bullet L^{-1} \bullet d^{-1}$, approximately three times higher than in the previous period. Specifically, the mass fluxes of individual VFAs were 7.56 ± 1.81 $gCOD \bullet m^{-2} \bullet h^{-1}$ for HAc, 0.81 ± 0.25 $gCOD \bullet m^{-2} \bullet h^{-1}$ for HPr and 0.44 ± 0.16 $gCOD \bullet m^{-2} \bullet h^{-1}$ for HBu. The increased flow produced a greater change in pH and conductivity (approximately two times higher than in the previous period) in the feed tank than in previous periods, confirming the increase in VFA transfer (Fig. 2(b)).

Consequently, the transfer efficiencies increased to 52 % ± 5 % for HAc, 39 % ± 3 % for HPr and 11 % ± 3 % for HBu (Fig. 2a). The higher OLR applied favoured the biomass growth observed by the increase of the concentration in the bioreactor. The highest value was obtained at 66 days, reaching 2.06 $gX_{PB} \bullet L^{-1}$ corresponding to a biomass production rate of 0.39 $gX_{PB} \bullet L^{-1} d^{-1}$. At the peak biomass concentration, the protein content was measured to be 61 %.

In parallel, the VFAs supplied through the MC were largely consumed, as confirmed by the low concentration of residual soluble COD in the effluent (500 mg•L⁻1, of which < 100 mgCODVFA•L⁻1) and a high COD removal efficiency of 94 %. This indicates that most of the transferred VFAs were effectively assimilated by PNSB biomass under the applied conditions.

The high OLR caused a pH decrease to 6.07 ± 0.21, mainly during the stripping phase, with the minimum recorded at the end of VFA loading. During the post-stripping phase, the pH slightly increased to 6.34 ± 0.18. At lower pH, the protonated form of VFAs becomes predominant, increasing their volatility and facilitating their transfer between phases. This shift in chemical speciation affects the partial pressure and diffusion of VFAs, which are crucial for maintaining the stability and functionality of the bioreactor.

The negative effect of the low pH is evident in the reduction of active biomass concentration, which dropped drastically from 2.06 $gX_{PB} \cdot L^{-1}$ (day 66) to 1.85 $gX_{PB} \cdot L^{-1}$ (day 72) (Fig. 2 (c)). Furthermore, it is important to highlight that, combined with the suboptimal pH, the rapid increase in biomass concentration within the AnPBR may have led to light attenuation, reducing the efficiency of light energy distribution throughout the culture volume and negatively affecting biomass growth rates (Puyol et al., 2019).

From day 75 to day 160 (period 4.2), the VFA transfer was decreased by shortening the stripping phase to 4 h (corresponding to 1.88 min contact time), with the feed temperature maintained at 32 ± 1°C. The total VFA flux remained consistent with the previous experimental period, measured at 8.86 g $COD \bullet m^{-2} \cdot h^{-1}$. This stability also applied to the individual acid fluxes: HAc, HPr, and HBu, which showed specific fluxes of 7.71, 0.77, and 0.38 $gCOD \cdot m^{-2} \cdot h^{-1}$, respectively (Fig. 2 (a)). The total VFA flux corresponded to an applied OLR of 3.9 ± 0.8 $gCOD \bullet L^{-1} \cdot d^{-1}$, nearly double that of Period 3, but still not high enough to induce significant pH fluctuations in the mixed liquor. During the VFAs loading phase, the pH stabilized around 6.6 ± 0.2, while in the effluent, it was 6.8 ± 0.2, remaining within the optimal range for PNSB growth. This facilitated the evaluation of long-term operational stability (75 days), as shown in (Fig. 2. (c)). Steady-state conditions were reached by day 90, where the active biomass concentration stabilized at 1.78 ± 0.05 $gX_{PB} \cdot L^{-1}$, with an active biomass production rate of 0.36 ± 0.01 $gX_{PB} \cdot L^{-1} \cdot d^{-1}$, 60 % higher than in Period 3.

The active biomass produced contained 62 % crude protein, with an output of almost 0.23 $gCP \cdot m^{-3} \cdot d^{-1}$. The total amino acid content increased from 469 $g \bullet kg^{-1}$ (Period 2) to 546 $g \bullet kg^{-1}$ (Period 4), resulting in an improved amino acid to crude protein ratio (AA/CP) from 80 % to 83 %. These values align with previous research, where crude protein content for PNSB biomass typically ranges from 45-65 % under various cultivation conditions (Capson-Tojo et al., 2020b; Hülsen et al., 2022b). The current CP value is at the high end of this range, highlighting the efficiency of the MC-AnPBR system in maximising protein synthesis and its potential for the sustainable production of protein-rich biomass.

Anaerobic conditions were maintained during the entire experimental period, confirmed by the absence of dissolved oxygen in the mixed liquor and a headspace composition of 97.2 % N_2, 2.5 % CO_2, 0.4 % O_2 and 0.01 % H_2. The average ORP of −195 mV during the stripping phase indicated a reductive, growth-promoting environment. Photoheterotrophic growth under these redox conditions is supported by the ability of the bacteria to maintain redox homeostasis through electron sink mechanisms such as PHA production.

These mechanisms help to manage the excess redox energy generated by the use of highly reduced carbon sources such as VFA. During the stripping phase, PHA accumulated in the biomass of PNSB at 6.1 % dry weight, with an HB:HV ratio of 2.7. In the post-stripping phase, when the carbon source became limited, PHA was consumed and decreased to 4.0 % (Table 4).

Beyond their role as electron sinks, PHAs are also valuable from a feed perspective: when included in aquafeeds, they stimulate the growth of probiotic bacteria (e.g., *Bacillus*, *Lactobacillus*, *Lactococcus*, *Bdellovibrio*) and enhance disease resistance, thereby improving fish health and survival (Asiri, 2024; Rodriguez-Estrada et al., 2021).

Several studies have shown that including 0.1–5 % PHAs in fish diets can reduce phenotype alterations and improve growth or feeding rates in species such as Kuruma shrimp, *Marsupenaeus japonicus*, and Nile tilapia, while also increasing protein digestibility (Asiri, 2024; Hülsen et al., 2022a; Rodriguez-Estrada et al., 2021).

Previous research (Allegue et al., 2022) reported a similar trend, with PHA accumulation decreasing from 42 % to 5 % dry weight as OLR increased from 1 $gCOD \bullet L^{-1} \bullet d^{-1}$ to 3 $gCOD \bullet L^{-1} \bullet d^{-1}$ indicating that organic overload negatively affects PHA synthesis (Allegue et al., 2022).

Table 3 shows the mass balance of carbon, nitrogen and phosphorus for different streams and transformation processes during the steady-state operation of the MC-AnPBR in Period 4.

Table 3. Mass balance of MC-AnPBR system derived from the experimental data obtained during Period 4. All values presented in the table are average values.

During Period 4.2, 87 % of the total COD fed into the system (6.16 $gCOD \cdot d^{-1}$) was removed, leaving 0.8 $gCOD \cdot d^{-1}$ as residual soluble COD in the effluent (Table 3). The removed COD was mainly converted into two primary products: PNSB biomass (1.86 $gCOD \cdot d^{-1}$, enriched in intracellular polymers) and gas production (mainly H_2 0.39 $gCOD \cdot d^{-1}$). This corresponded to an observed biomass yield (Y_{obs}) of 0.36 $gCOD_X \cdot gCOD^{-1}$ (Fig. 4).

However, the nutrient solution is the main source of essential nutrients, contributing 0.11 $gN \bullet d^{-1}$ of nitrogen and 0.20 $gP \bullet d^{-1}$ of phosphorus. The biomass produced in the system incorporates carbon, nitrogen, and phosphorus in ratios that reflect the metabolic demands of

Table 3
Mass balance of MC-AnPBR system derived from the experimental data obtained during Period 4. All values presented in the table are average values.

Influent	COD $gCOD \cdot d^{-1}$	TN $gN \cdot d^{-1}$	TP $gP \cdot d^{-1}$
Gaseous VFA stream	6.10	0	0
Nutrient solution	0.06*	0.11	0.20
Total Streams influent	6.16	0.11	0.20
Effluent	**COD** $gCOD \cdot d^{-1}$	**TN** $gN \cdot d^{-1}$	**TP** $gP \cdot d^{-1}$
Supernatant soluble	0.8	0.01	0.04
PNSB suspended biomass	1.86	0.10	0.10
H_2	0.39	0	0
Calculated Parameters			
Removal efficiencies %	87	91	80

*Yeast extract was estimated to be 40% organic carbon and contribute to 0.81 $mgCOD\ mg_{YE}^{-1}$, while nitrogen was estimated to be 20% and 2.8 % of Phosphorus (Thompson et al., 2017).

Table 4
Characterization of Single Cell Protein (SCP) and quality.

Parameters	Unit	Period 2	Period 3	Period 4
MLVSS	$kg \cdot m^{-3}$	0.59 ± 0.22	1.09 ± 0.07	1.87 ± 0.05
Crude Protein	$g \cdot kg_{MLVSS}^{-1}$	515 ± 2.06	541 ± 2.10	624 ± 2.31
Aminoacids	$g \cdot kg_{MLVSS}^{-1}$	469 ± 2.06	490 ± 2.10	546 ± 2.31
Tot. BChls	$g_{BChls} \cdot kg_{MLVSS}^{-1}$	10.2 ± 0.26	8.39 ± 0.03	12.1 ± 0.14
Tot. Carotenoids	$g_{Crts} \cdot kg_{MLVSS}^{-1}$	1.08 ± 0.05	2.29 ± 0.03	2.79 ± 0.02
PHA	$g \cdot kg_{MLVSS}^{-1}$	120 ± 12	90 ± 5	40 ± 12
SCP Quality %	$gBioP^* \cdot g_{MLVSS}^{-1}$	65 ± 2.9 (52 %CP; 1 %Pigm.; 12 %PHA)	64 ± 1.4 (54 %CP; 1 %Pigm.; 9 %PHA)	68 ± 2.9 (62 %CP; 1 %Pigm.; 4 %PHA)

*Bioproduct in term of Crude Protein, Pigments (BChls + Crts) and PHA.

PNSB under photoheterotrophic condition, typically with a ratio of COD:N:P = 100:(6.7–12):(0.9–12) (Capson-Tojo et al., 2021).

The relatively low observed yield can be attributed to the omission of attached biofilm biomass, which was not considered but may account for 30–75 % of COD uptake in PNSB systems (Capson-Tojo et al., 2020b; Hülsen et al., 2022a). It should also be noted that yields from pure PPB cultures are not always higher and, in some cases, approach those typically observed in mixed cultures or activated sludge systems (~0.5 gCOD/gCOD removed; Henze et al., 2002; Capson-Tojo et al., 2022).

In addition, approximately 91 % of the nitrogen in the nutrient solution was assimilated into the biomass, resulting in a protein production efficiency of 0.12 $gN\text{-}Prot \cdot gCOD^{-1}_{removed}$. The observed levels of phosphorus in the biomass reflect (13.3 % dry matter) these critical functions, with a proportion contributing to polyphosphate storage, which can account for up to 13–15 % of cell dry weight in certain strains during stationary growth (Lai et al., 2017). The hydrogen production rate, based on a conversion factor of 8 $gCOD \cdot gH_2^{-1}$ (Huang et al., 2025), was calculated considering the flow rate of vacuum pump (0.7 $m^3 \cdot h^{-1}$) and a hydrogen concentration of 0.013 %. With a stripping time of 6 h per day, the system produced 0.55 $LH_2 \cdot d^{-1}$. This corresponds to a specific hydrogen production of 0.05 $gCODH_2 \cdot gCOD^{-1}$ removed or a volumetric yield of 0.10 $LH_2 \cdot gCOD^{-1}$ removed.

3.2. Microbial analysis of the anaerobic photobioreactor

The dominance of PNSB was detected in all the experimental periods, although their abundances and the coexistence of other species were mainly related to the variation of the pH in the mixed liquor observed under the different OLR applied in the AnPBR. On day 7 of the preliminary test, the predominance of *Xanthobacteraceae* family (PNSB) was measured at 80.4 % (Fig. 3). The main genus was *Rhodopseudomonas sp.*, thus confirming the good acclimatization of the inoculum.

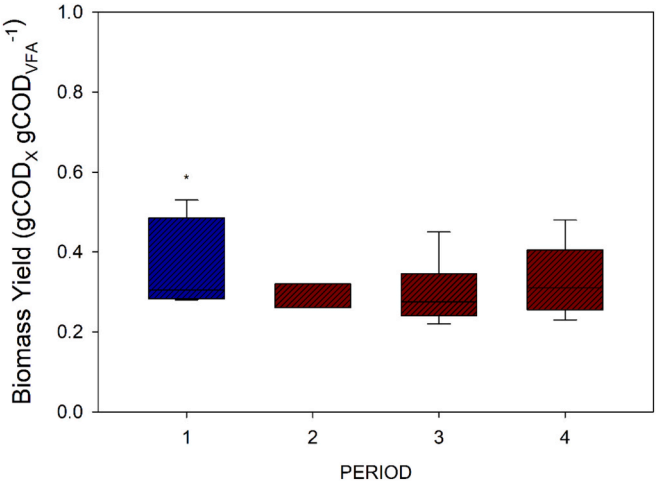

Fig. 4. Biomass yield ($gCOD \bullet gCOD^{-1}$) in the different periods *biomass yield during contamination.

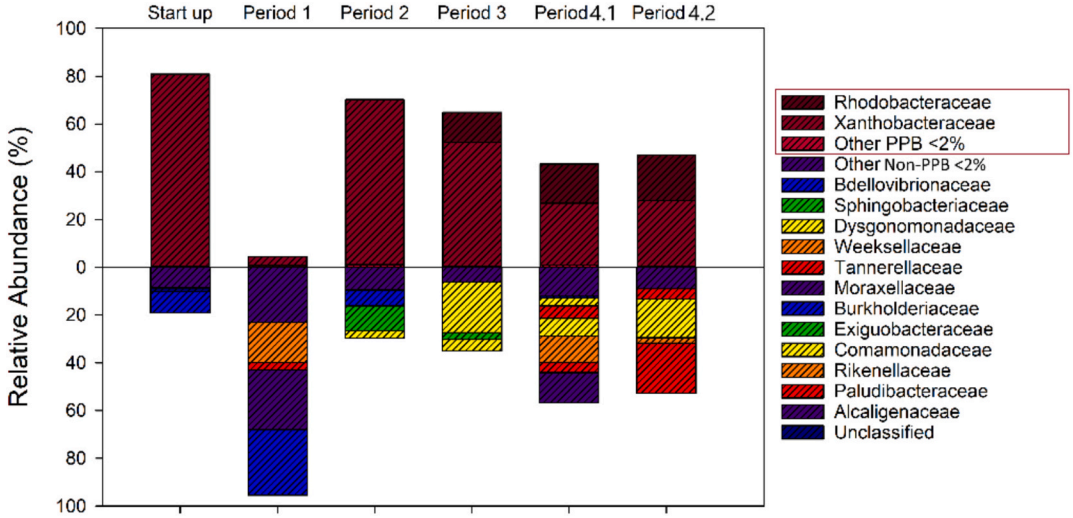

Fig. 3. Microbial community structure expressed as relative abundance of family-level taxa in the AnPBR biomass over different experimental periods.

In Period 1, a decrease in the relative abundance of PNSB families equal to 4.46 % was measured due to not optimal conditions of the bioreactor reported in Section 3.1.1. Conversely, an enrichment in aerobic species belonging to the following families was measured: *Burkholderiaceae* (27.51 %), *Moraxellaceae* (25.2 %) and *Weeksellaceae* (16.95 %).

From Periods 2 to 4, the increase of the VFAs led to a higher variation of the pH value in the effluent which had an influence in the microbial community. These conditions facilitated the growth of different communities depending on their tolerance of different pH levels.

During Period 2, the pH of the mixed liquor was close to neutrality (see supporting material), resulting in favorable growth conditions that maintained the relative abundance of PNSB families above 70 % (sampled at day 43). Whitin this group, *Xanthobacteraceae* accounted for up to 69 %, of which 98.7 % corresponded to *Rhodopseudomonas* sp. Among non-PNSB families detected in the AnPBR (29 %), *Sphingobacteriaceae* were the most abundant, representing 10.4 %. Their presence can be attributed to growth conditions that supported anaerobiosis and a pH range from neutral to moderately alkaline (Wang et al., 2021).

In Period 3, the operating changes did not significantly affect the pH of the mixed liquor compared to Period 2 (see supporting material), allowing PNSB to remain dominant at 64.9 % of the biomass (sampled at day 63). Of these, 75 % were *Xanthobacteraceae* and 20 % *Rhodobacteraceae* (Fig. 3). Among non-PNSB families, *Dysgonomonadaceae* were the most abundant (21 %), but their levels remained stable, consistent with their adaptation to neutral or slightly alkaline pH conditions for their growth (Owusu-Agyeman et al., 2022).

Unlike the previous periods, Period 4 was marked mainly by a higher VFA transfer rate, which led to acidic pH value of the mixed liquor, typically lower than 6.5 during the VFA loading phase. As result, in this Period, it was observed a reduction of approximately 15 % in the PNSB community abundance compared to Period 2 (Fig. 3). In particular, the dominant family was *Xanthobacteraceae* (27.5 %) followed by the *Rhodobacteraceae* family (~20 %) with *Rhodopseudomonas* sp. and *Rhodobacter* sp. being the dominant genera. Consequently, an increase was observed in non-PSNB families adapted to grow at acidic pH in a range between 5.5 and 7.5 (Gronow et al., 2011), such as the *Paludibacteraceae* family, which achieved a relative abundance of 21 %.

3.3. Dynamics of pigment concentrations over experimental periods

At the end of Preliminary test, the content of BChl and carotenoids produced under anaerobically illuminated conditions during photoheterotrophic growth was respectively 14.19 ± 1.65 mg·gMLVSS^{-1} and 1.45 ± 0.01 g·gMLVSS^{-1}. During Period 1, pigment analysis revealed a decrease in PNSB biomass compared to aerobic species, specifically a carotenoids content of 0.48 ± 0.05 g•kgMLVSS^{-1} were measured, significantly lower than typical range for PNSB (0.5 to > 12 g•kgVS^{-1}) (Grassino et al., 2022; Hülsen et al., 2022a). Similarly, BChl content was 2.59 ± 0.21 g•kgMLVSS^{-1}, approximately 4 to 8 times lower than the reported values for PNSB (10–20 g•kg^{-1}) (Hülsen et al., 2022a). This reduction was attributed to both the decreased of the relative abundance of PNSB and the inhibition of pigment synthesis due to the presence of dissolved oxygen in the bioreactor (Capson-Tojo et al., 2021). The total pigments concentration in biomass during Period 1 was about 4.5 times lower than the levels obtained in Period 2, likely due to the presence of dissolved oxygen in the mixed liquor.

From Period 2 to Period 4, both bacteriochlorophylls (BChl) and carotenoids (Crts) showed an overall increasing trend approximately in line with the OLR trend applied (Table 4), indicating improved pigment production under optimized conditions. In Period 2, anaerobic conditions and NIR illumination promoted the synthesis of BChl and carotenoids, particularly in *R. palustris* sp. These pigments essential for cell homeostasis and growth, reached concentrations of BChl and Crts respectively of 10.20 ± 0.27 g_{BChl}·kgMLVSS^{-1} and 1.08 ± 0.05g_{Crts}·kgMLVSS^{-1} in line with the expected range under PNSB-photoheterotrophic growth condition. The absence of oxygen in the bioreactor prevented pigment synthesis inhibition, leading to a ~ 75 % increase (Kojadinovic et al., 2008). The formation of photosynthetic apparatus and pigment production are regulated by both oxygen concentration, light quality and intensity; when oxygen exceeds 8 %, synthesis is suppressed, whereas NIR light under anaerobic conditions stimulates production (Kojadinovic et al., 2008).

By Period 3, total pigment content accounted for 11.7 % of MLVSS comparable with the Period 2, despite slight variation in BChl of 8.39 ± 0.03g_{BChl}·kgMLVSS^{-1} and in Crts of 2.29 ± 0.03g_{Crts}·kgMLVSS^{-1}. These value align with previous study linking pigment production to the synthesis of light-harvesting complexes (LH1, LH2) under NIR illumination (Liu, 2016).

At the beginning of Period 4, BChl and Crts concentrations slightly dropped respectively by 12 % to 9.46 ± 0.28 g_{BChl}·kgMLVSS^{-1} and of the carotenoids by 8 % to 2.25 ± 0.05gCrts·kgMLVSS^{-1}, compared to Period 3. Despite suboptimal conditions for biomass growth, pigment levels remained significant, consisted with the literature indicating that anaerobic conditions support pigment production even under acidic stress (Nasha Musa and Zulaikha Yusof, 2019). Additionally, PNSB regulate their photosynthetic stoichiometry according to light intensity. Under low light, they increase LHCs numbers to maximise photon capture, while at high intensities, LHC levels decrease to prevent excess energy absorption and photo-damage (Harada et al., 2008).

At the end of the Period 4, the reductive environment along with the NIR illumination in the bioreactor also prevents inhibition of pigment production and ensuring continued photosynthetic activity (Capson-Tojo et al., 2020). In line with the OLR applied in this Period, the highest levels of BChl and carotenoids levels were measured, respectively of 12.10 ± 0.14 g_{BChl}•kgMLVSS^{-1} and of 2.79 ± 0.02 gCrts•kgMLVSS^{-1}, which aligning with the results of other studies on PNSB pigment production in the photoheterotrophic mode (Grassino et al., 2022; Yu et al., 2021).

In addition to their metabolic role, carotenoids provide functional benefits in aquaculture by enhancing fish pigmentation, boosting immune responses, and improving overall growth performance. The carotenoid content in PNSB biomass (500–13000 mg kg^{-1} dry biomass) is markedly higher than typical aquafeed supplementation levels (50–100 mg kg^{-1}) (Alloul et al., 2021; González Cámara et al., 2025), suggesting that even limited inclusion of PNSB in feed could meet or exceed carotenoid dietary requirements in aquaculture.

3.4. Amino acids profile of the single cell protein

The amino acid content of the biomass showed a progressive improvement from Period 2 to Period 3 (see supporting material), with total amino acids increasing from 469 g·kgMLVSS^{-1} to 490 g·kgMLVSS^{-1} (Table 4) reflecting a 4.5 % increase in protein synthesis, these values are within the expected range for the PNSB community (405–585 g·kgMLVSS^{-1}) (Capson-Tojo et al., 2020b; Hülsen et al., 2022a), reflecting a 4.5 % increase in protein synthesis. Among the most abundant amino acids in both periods were L-aspartic acid (from 52.0 to 54.5 g·kg^{-1}), L-glutamic acid (from 50.0 to 52.3 g·kg^{-1}) and L-leucine (from 42.8 to 44.8 g·kg^{-1}), which are crucial for protein structure and metabolism. In addition, essential amino acids such as L-lysine (from 46.0 to 48.1 g·kg^{-1}) and L-threonine (from 20.6 to 21.6 g·kg^{-1}) also increased, further enhancing the nutritional quality of the biomass. The biomass produced in the Period 4 under steady-state conditions was characterized in terms of the protein content and the amino acid composition using the Chemical Score (CS) method (see Section 2.4.4). Fig. 5 shows the relative abundances of essential amino acids (EAA) in the SCP compared to conventional fishmeal and other protein-rich feeds. Key amino acids such as L-Lysine (53.6 g·kg^{-1}), L-Leucine (49.9 g·kg^{-1}) and L-Isoleucine (29.1 g·kg^{-1}) showed CS values above 100 % (threshold), indicating that these EAA are present in sufficient quantities to meet or exceed the dietary requirements of aquaculture species such as Tilapia

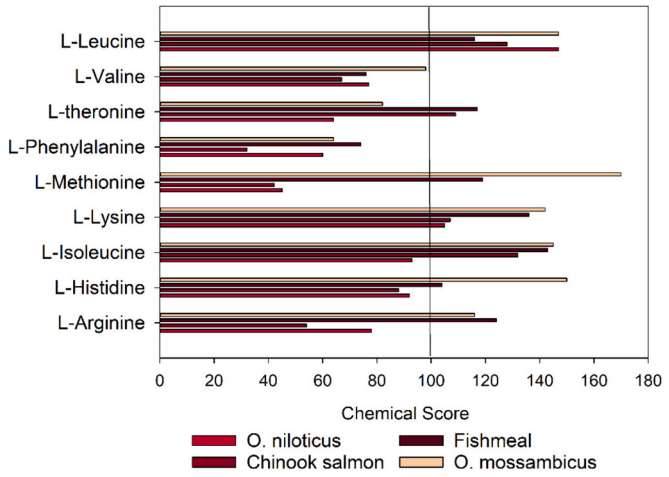

Fig. 5. Chemical score of essential amino acids (EAAs) in the produced biomass compared with the dietary requirements of aquaculture species (*Oreochromis niloticus*, *Oreochromis mossambicus, Chinook salmon*) and fishmeal.

(*Oreochromis niloticus*) and Chinook salmon. The concentrations of these three EAA in the produced biomass exceeded those reported by (Hülsen et al., 2020) for the PNSB grown in suspended configurations, with L-Lysine, L-Leucine and L-Isoleucine higher of 48 %, 16 %, and 14 %, respectively. Furthermore, the concentrations of L-Leucine and L-Threonine in the present study were 82 % and 78 % higher, respectively, compared to those found in *Chlorella* sp. algal biomass (Hülsen et al., 2018). L-Valine, a common limiting EAA in plant-based diets, showed a CS of less than 100 %, highlighting the need for Valine supplementation when using this biomass as the sole feed ingredient. Similarly, L-Methionine and L-Phenylalanine were slightly underrepresented compared to the dietary requirements of the target species. Despite these minor limitations, the overall EAA profile closely matches the dietary requirements of aquaculture species, confirming the potential of biomass as a viable alternative protein source.

Besides its high crude protein content (~ 60 %) and high protein quality, the biomass produced in the MC-AnPBR also contained secondary metabolites, such as carotenoids and bacteriochlorophylls and PHAs, accounting for approximately 10 % of the biomass (Table 4). These compounds have been shown to be important bioactive substances with immunomodulatory effects in animals (Liu, 2016).

The high-quality of SCP composition not only confirms the high performance of the MC-AnPBR system but also results from the system's specific operation. By transferring VFAs from the fermentation liquid solution to the gaseous phase, the MC system minimises the input of non-biodegradable COD (nbCOD) and inert materials in the biomass of the AnPBR, ensuring a higher proportion of active and functional components in the biomass. For example, the MC-AnPBR system produced suspended biomass with > 95 % VS/TS as inert material, whereas a system involving batch test produced suspended biomass with up to 62 % VS/TS as inert material (Hülsen et al., 2018). This further supports the suitability of the proposed system as a practical and sustainable solution for the production of alternative proteins, particularly for use in the animal feed industry.

4. Conclusions

The study investigated the feasibility of continuous production of single cell protein in an anaerobic photobioreactor using a gaseous stream of volatile fatty acids transferred from the synthetic fermented broth through a membrane contactor. This novel approach avoids direct contact between the fermented broth and the biomass, ensuring a cleaner and controlled protein production process. Over an experimental period of 160 days, the system was optimised in four operational steps to achieve high biomass yields and single cell protein quality under different organic loading rates. Under these optimised conditions, the photobioreactor demonstrated consistent performance, achieving a biomass production rate of 0.36 $kgX_{PB}·m^{-3}·d^{-1}$ with protein content of 62 %. The amino acid profile of the biomass closely matched the aquaculture species and commercial fishmeal dietary requirements. This strategy shows the process's potential to support circular bioeconomy practices, contribute to European Union environmental goals and promote innovative, low-impact alternatives for animal feed production.

CRediT authorship contribution statement

Riccardo Lo Coco: Writing – review & editing, Writing – original draft, Visualization, Validation, Software, Methodology, Investigation, Formal analysis, Data curation, Conceptualization. **Marco Pezzuto:** Writing – review & editing, Writing – original draft, Visualization, Software, Methodology, Investigation, Formal analysis, Data curation, Conceptualization. **Aleksandra Jelic:** Writing – review & editing, Writing – original draft, Validation. **Stefano Cazzaniga:** Data Curation, Writing – original draft, Investigation. **Nicola Frison:** Writing – review & editing, Writing – original draft, Supervision, Resources, Funding acquisition.

Declaration of competing interest

The authors declare that they have no known competing financial interests or personal relationships that could have appeared to influence the work reported in this paper.

Acknowledgements

The authors gratefully acknowledge the funding received for the PhD scholarship, supported by FSE REACT-EU resources on Green and Innovation topics under the National Operational Programme for Research and Innovation 2014–2020 (Azione IV.5, "Dottorati su tematiche green", CUP B39J21025820001). This study was also supported by the project PHARPLE – Sustainable PHA recovery from agri-food waste via purple non-sulfur bacteria mixed cultures, funded by the Italian Ministry of University and Research (PNRR per la Missione 4, Componente 2, investimento 1.1., finanziato dall'Unione europea – NextGenerationEU. Progetto: 2022MHBMEH - CUP: B53D23006260001). The authors would like to thank Davide Bertasini for his valuable contribution to the design of the Graphical Abstract, which effectively illustrates the key concepts of this study.

Appendix A. Supplementary data

Supplementary data to this article can be found online at https://doi.org/10.1016/j.biortech.2025.133413.

Data availability

Data will be made available on request.

References

Adesogan, A.T., Havelaar, A.H., McKune, S.L., Eilittä, M., Dahl, G.E., 2020. Animal source foods: Sustainability problem or malnutrition and sustainability solution? Perspective matters. Glob. Food Sec. 25, 100325. https://doi.org/10.1016/J.GFS.2019.100325.

Allegue, L.D., Ventura, M., Melero, J.A., Puyol, D., 2022. Unraveling PHA production from urban organic waste with purple phototrophic bacteria via organic overload. Renew. Sustain. Energy Rev. 166. https://doi.org/10.1016/j.rser.2022.112687.

Alloul, A., Ganigué, R., Spiller, M., Meerburg, F., Cagnetta, C., Rabaey, K., Vlaeminck, S. E., 2018. Capture-ferment-upgrade: a three-step approach for the valorization of sewage organics as commodities. Environ. Sci. Technol. 52, 6729–6742. https://doi.org/10.1021/ACS.EST.7B05712.

Alloul, A., Wille, M., Lucenti, P., Bossier, P., Van Stappen, G., Vlaeminck, S.E., 2021. Purple bacteria as added-value protein ingredient in shrimp feed: Penaeus vannamei

growth performance, and tolerance against Vibrio and ammonia stress. Aquaculture 530, 735788. https://doi.org/10.1016/J.AQUACULTURE.2020.735788.
Ángeles, R., Carvalho, J., Hernández-Martínez, I., Morales-Ibarría, M., Fradinho, J.C., Reis, M.A.M., Lebrero, R., 2025. Harnessing nature's palette: exploring photosynthetic pigments for sustainable biotechnology. N. Biotechnol. 85, 84–102. https://doi.org/10.1016/J.NBT.2025.01.001.
Asiri, F., 2024. Polyhydroxyalkanoates for sustainable aquaculture: a review of recent advancements, challenges, and future directions. J. Agric. Food Chem. 72, 2034–2058. https://doi.org/10.1021/ACS.JAFC.3C06488.
Atasoy, M., Owusu-Agyeman, I., Plaza, E., Cetecioglu, Z., 2018. Bio-based volatile fatty acid production and recovery from waste streams: current status and future challenges. Bioresour. Technol. 268, 773–786. https://doi.org/10.1016/J.BIORTECH.2018.07.042.
Aydin, S., Yesil, H., Tugtas, A.E., 2018. Recovery of mixed volatile fatty acids from anaerobically fermented organic wastes by vapor permeation membrane contactors. Bioresour. Technol. 250, 548–555. https://doi.org/10.1016/j.biortech.2017.11.061.
Bond-Watts, B.B., Bellerose, R.J., Chang, M.C.Y., 2011. Enzyme mechanism as a kinetic control element for designing synthetic biofuel pathways. Nat. Chem. Biol. 7, 222–227. https://doi.org/10.1038/NCHEMBIO.537.
Braunegg, G., Sonnleitner, B., Lafferty, R.M., 1978. A rapid gas chromatographic method for the determination of poly-β-hydroxybutyric acid in microbial biomass. Eur. J. Appl. Microbiol. Biotechnol. 6, 29–37. https://doi.org/10.1007/BF00500854/METRICS.
Capson-Tojo, G., Batstone, D.J., Grassino, M., Vlaeminck, S.E., Puyol, D., Verstraete, W., Kleerebezem, R., Oehmen, A., Ghimire, A., Pikaar, I., Lema, J.M., Hülsen, T., 2020. Purple phototrophic bacteria for resource recovery: challenges and opportunities. Biotechnol. Adv. https://doi.org/10.1016/j.biotechadv.2020.107567.
Capson-Tojo, G., Lin, S., Batstone, D.J., Hülsen, T., 2021. Purple phototrophic bacteria are outcompeted by aerobic heterotrophs in the presence of oxygen. Water Res. 194. https://doi.org/10.1016/j.watres.2021.116941.
Cazzaniga, S., Perozeni, F., Baier, T., Ballottari, M., 2022. Engineering astaxanthin accumulation reduces photoinhibition and increases biomass productivity under high light in Chlamydomonas reinhardtii. Biotechnol. Biofuels Bioprod. 15, 1–17. https://doi.org/10.1186/S13068-022-02173-3/FIGURES/7.
Chazaux, M., Schiphorst, C., Lazzari, G., Caffarri, S., 2022. Precise estimation of chlorophyll a, b and carotenoid content by deconvolution of the absorption spectrum and new simultaneous equations for Chl determination. Plant J. 109, 1630–1648. https://doi.org/10.1111/TPJ.15643.
Delamare-Deboutteville, J., Batstone, D.J., Kawasaki, M., Stegman, S., Salini, M., Tabrett, S., Smullen, R., Barnes, A.C., Hülsen, T., 2019. Mixed culture purple phototrophic bacteria is an effective fishmeal replacement in aquaculture. Water Res. X 4. https://doi.org/10.1016/j.wroa.2019.100031.
Frison, N., Katsou, E., Malamis, S., Oehmen, A., Fatone, F., 2015. Development of a novel process integrating the treatment of sludge reject water and the production of polyhydroxyalkanoates (PHAs). Environ. Sci. Technol. 49, 10877–10885. https://doi.org/10.1021/acs.est.5b01776.
González Cámara, S.J., Kibor, S., Olyslaegers, S., Alloul, A., Allegue, L.D., De Boeck, G., Vlaeminck, S.E., 2025. Purple bacteria as sustainable nutraceutical ingredient in aquafeed: the case of guppies. Anim. Feed Sci. Technol. 326, 116394. https://doi.org/10.1016/J.ANIFEEDSCI.2025.116394.
Grassino, M., Batstone, D.J., Yong, K.W.L., Capson-Tojo, G., Hülsen, T., 2022. Method development for PPB culture screening, pigment analysis with UPLC-UV-HRMS vs. spectrophotometric methods, and spectral decomposition-based analysis. Talanta 246, 123490. https://doi.org/10.1016/J.TALANTA.2022.123490.
Gronow, S., Munk, C., Lapidus, A., Nolan, M., Lucas, S., Hammon, N., Deshpande, S., Cheng, J.F., Tapia, R., Han, C., Goodwin, L., Pitluck, S., Liolios, K., Ivanova, N., Mavromatis, K., Mikhailova, N., Pati, A., Chen, A., Palaniappan, K., Land, M., Hauser, L., Chang, Y.J., Jeffries, C.D., Brambilla, E., Rohde, M., Göker, M., Detter, J. C., Woyke, T., Bristow, J., Eisen, J.A., Markowitz, V., Hugenholtz, P., Kyrpides, N.C., Klenk, H.P., 2011. Complete genome sequence of Paludibacter propionicigenes type strain (WB4T). Stand Genomic Sci. 4, 36. https://doi.org/10.4056/SIGS.1503846.
Harada, J., Mizoguchi, T., Yoshida, S., Isaji, M., Oh-Oka, H., Tamiaki, H., 2008. Composition and localization of bacteriochlorophyll a intermediates in the purple photosynthetic bacterium Rhodopseudomonas sp. Rits. Photosynth Res 95, 213–221. https://doi.org/10.1007/S11120-007-9254-1.
Hasanoğlu, A., Romero, J., Pérez, B., Plaza, A., 2010. Ammonia removal from wastewater streams through membrane contactors: experimental and theoretical analysis of operation parameters and configuration. Chem. Eng. J. 160, 530–537. https://doi.org/10.1016/j.cej.2010.03.064.
Huang, P., Chen, Y., Yu, S., Zhou, Y., 2025. Propionic acid enhances H2 production in purple phototrophic bacteria: Insights into carbon and reducing equivalent allocation. Water Res. 269, 122799. https://doi.org/10.1016/J.WATRES.2024.122799.
Hülsen, T., Barnes, A.C., Batstone, D.J., Capson-Tojo, G., 2022a. Creating value from purple phototrophic bacteria via single-cell protein production. Curr. Opin. Biotechnol. 76, 102726. https://doi.org/10.1016/J.COPBIO.2022.102726.
Hülsen, T., Hsieh, K., Lu, Y., Tait, S., Batstone, D.J., 2018. Simultaneous treatment and single cell protein production from agri-industrial wastewaters using purple phototrophic bacteria or microalgae - a comparison. Bioresour. Technol. 254, 214–223. https://doi.org/10.1016/J.BIORTECH.2018.01.032.
Hülsen, T., Sander, E.M., Jensen, P.D., Batstone, D.J., 2020. Application of purple phototrophic bacteria in a biofilm photobioreactor for single cell protein production: biofilm vs suspended growth. Water Res. 181, 115909. https://doi.org/10.1016/J.WATRES.2020.115909.
Hülsen, T., Stegman, S., Batstone, D.J., Capson-Tojo, G., 2022b. Naturally illuminated photobioreactors for resource recovery from piggery and chicken-processing wastewaters utilising purple phototrophic bacteria. Water Res. 214, 118194. https://doi.org/10.1016/J.WATRES.2022.118194.
Kaya, E., Hasanoğlu, A., 2022. Removal of acetic acid from aqueous post-fermentation streams and fermented beverages using membrane contactors. J. Chem. Technol. Biotechnol. 97, 2218–2230. https://doi.org/10.1002/jctb.7100.
Kojadinovic, M., Laugraud, A., Vuillet, L., Fardoux, J., Hannibal, L., Adriano, J.M., Bouyer, P., Giraud, E., Verméglio, A., 2008. Dual role for a bacteriophytochrome in the bioenergetic control of Rhodopsdeudomonas palustris: Enhancement of photosystem synthesis and limitation of respiration. Biochimica et Biophysica Acta (BBA) - Bioenergetics 1777, 163–172. https://doi.org/10.1016/J.BBABIO.2007.09.003.
Lai, Y.C., Liang, C.M., Hsu, S.C., Hsieh, P.H., Hung, C.H., 2017. Polyphosphate metabolism by purple non-sulfur bacteria and its possible application on photo-microbial fuel cell. J. Biosci. Bioeng. 123, 722–730. https://doi.org/10.1016/J.JBIOSC.2017.01.012.
Liu, L.N., 2016. Distribution and dynamics of electron transport complexes in cyanobacterial thylakoid membranes. Biochimica et Biophysica Acta (BBA) - Bioenergetics 1857, 256–265. https://doi.org/10.1016/J.BBABIO.2015.11.010.
Liu, S., Zhang, G., Zhang, J., Li, X., Li, J., 2016. Performance, 5-aminolevulinic acid (ALA) yield and microbial population dynamics in a photobioreactor system treating soybean wastewater: effect of hydraulic retention time (HRT) and organic loading rate (OLR). Bioresour. Technol. 210, 146–152. https://doi.org/10.1016/J.BIORTECH.2016.01.030.
Lo Coco, R., Jelic, A., Järvelä, E., Frison, N., 2024. Recovery of bio-based volatile fatty acids from anaerobically treated winery wastewater using a closed-loop liquid-liquid hydrophobic membrane contactor system. Chem. Eng. J. 500, 156889. https://doi.org/10.1016/J.CEJ.2024.156889.
Matassa, S., Batstone, D.J., Hülsen, T., Schnoor, J., Verstraete, W., 2015. Can direct conversion of used nitrogen to new feed and protein help feed the world? Environ. Sci. Technol. 49, 5247–5254. https://doi.org/10.1021/ES505432W/ASSET/IMAGES/LARGE/ES-2014-05432W_0002.JPEG.
McKinlay, J.B., Harwood, C.S., 2011. Calvin cycle flux, pathway constraints, and substrate oxidation state together determine the H2 biofuel yield in photoheterotrophic bacteria. mBio 2. https://doi.org/10.1128/MBIO.00323-10.
Nasha Musa, N., Zulaikha Yusof, N., 2019. Chemical and physical parameters affecting bacterial pigment production. Mater. Today Proc. 19, 1608–1617. https://doi.org/10.1016/J.MATPR.2019.11.189.
Owusu-Agyeman, I., Plaza, E., Cetecioglu, Z., 2022. Long-term alkaline volatile fatty acids production from waste streams: Impact of pH and dominance of Dysgonomonadaceae. Bioresour. Technol. 346, 126621. https://doi.org/10.1016/J.BIORTECH.2021.126621.
Pervez, M.N., Mahboubi, A., Uwineza, C., Zarra, T., Belgiorno, V., Naddeo, V., Taherzadeh, M.J., 2022. Factors influencing pressure-driven membrane-assisted volatile fatty acids recovery and purification-a review. Sci. Total Environ. https://doi.org/10.1016/j.scitotenv.2022.152993.
Pesante, G., Bolzonella, D., Jelic, A., Frison, N., 2024. Upgrading biogas plants to produce microbial proteins for aquaculture feed. J. Clean. Prod. 459, 142559. https://doi.org/10.1016/J.JCLEPRO.2024.142559.
Pikaar, I., Matassa, S., Rabaey, K., Bodirsky, B.L., Popp, A., Herrero, M., Verstraete, W., 2017. Microbes and the next nitrogen revolution. Environ. Sci. Technol. 51, 7297–7303. https://doi.org/10.1021/ACS.EST.7B00916/ASSET/IMAGES/LARGE/ES-2017-00916X_0003.JPEG.
Puyol, D., Monsalvo, V.M., Marin, E., Rogalla, F., Melero, J.A., Martínez, F., Hülsen, T., Batstone, D.J., 2019. Purple phototrophic bacteria as a platform to create the next generation of wastewater treatment plants: energy and resource recovery. Wastewater Treatment Residues as Resources for Biorefinery Products and Biofuels 255–280. https://doi.org/10.1016/B978-0-12-816204-0.00012-6.
Righetti, E., Nortilli, S., Fatone, F., Frison, N., Bolzonella, D., 2020. A Multiproduct biorefinery approach for the production of hydrogen, methane and volatile fatty acids from agricultural waste. Waste Biomass Valoriz. 11, 5239–5246. https://doi.org/10.1007/s12649-020-01023-3.
Rodriguez-Estrada, U., Tachibana, L., de Carla Dias, D., Ben-Hamed, S., Sampaio-Goncalves, G., Rosa Sussel, F., Ranzani-Paiva, M.J., 2021. Dietary pure polyhydroxyalkanoate effects on growth, nutrient utilization, apparent digestibility, and hematology in Nile Tilapia. N. Am. J. Aquac. 83, 240–254. https://doi.org/10.1002/NAAQ.10183.
Sepúlveda-Muñoz, C.A., Ángeles, R., de Godos, I., Muñoz, R., 2020. Comparative evaluation of continuous piggery wastewater treatment in open and closed purple phototrophic bacteria-based photobioreactors. J. Water Process Eng. 38, 101608. https://doi.org/10.1016/J.JWPE.2020.101608.
Strazzera, G., Battista, F., Garcia, N.H., Frison, N., Bolzonella, D., 2018. Volatile fatty acids production from food wastes for biorefinery platforms: a review. J. Environ. Manage. 226, 278–288. https://doi.org/10.1016/j.jenvman.2018.08.039.
Takahashi, S., Tomita, J., Nishioka, K., Hisada, T., Nishijima, M., 2014. Development of a prokaryotic universal primer for simultaneous analysis of Bacteria and Archaea using next-generation sequencing. PLoS One 9. https://doi.org/10.1371/JOURNAL.PONE.0105592.
Tugtas, A.E., 2014. Recovery of volatile fatty acids via membrane contactor using flat membranes: experimental and theoretical analysis. Waste Manag. 34, 1171–1178. https://doi.org/10.1016/j.wasman.2014.01.020.
Wada, O.Z., Vincent, A.S., Mackey, H.R., 2022. Single-cell protein production from purple non-sulphur bacteria-based wastewater treatment. In: Reviews in

Environmental Science and Bio/technology. https://doi.org/10.1007/S11157-022-09635-Y.

Wang, Y., Brons, J.K., van Elsas, J.D., 2021. Considerations on the identity and diversity of organisms affiliated with sphingobacterium multivorum—proposal for a new species, sphingobacterium paramultivorum. Microorganisms 9, 2057. https://doi.org/10.3390/MICROORGANISMS9102057/S1.

Yesil, H., Calli, B., Tugtas, A.E., 2021. A hybrid dry-fermentation and membrane contactor system: enhanced volatile fatty acid (VFA) production and recovery from organic solid wastes. Water Res. 192. https://doi.org/10.1016/j.watres.2021.116831.